Locating reactive groups on nanomaterials with gold nanoclusters – towards a surface reactive site map

Steffi S. Thomas, Matthew Coleman, Emma Carrol, Ester Polo, Fabian Meder, Kenneth A. Dawson**

Centre for BioNano Interactions, University College Dublin, School of Chemistry and Chemical Biology, Belfield, Dublin 4, Ireland.

Correspondence should be addressed to Kenneth A. Dawson (kenneth.a.dawson@cbni.ucd.ie) or Fabian Meder (mederf@gmx.de)

KEYWORDS

Silica nanoparticles, thiolation, amination, functional groups, gold nanoclusters, mapping, microscopy.

ABSTRACT

Nanoparticles (NPs) are often functionalized with reactive groups like amines or thiols for the subsequent conjugation of further molecules, *e.g*., stabilizing polymers, drugs and proteins for targeting cells or specific diseases, *etc*. In addition to the quantitative estimation of the reactive conjugation sites, their nanoscale and molecular positioning and local arrangement on single nanoparticles becomes more and more important for tailored engineering and design of functional nanomaterials. Here, we use maleimide or sulfo-succinimidyl ester modified 1.4 nm gold nanoclusters (AuNCs) to specifically label reactive thiol and amine groups with sub – 2 nm precision on metal oxide and polymeric nanostructures. We confirm the binding of AuNCs by measuring and modelling sedimentation properties using analytical centrifugation, image their surface distribution and surface distances by transmission electron microscopy (TEM), and compare the results to ensemble measurements of numbers of reactive surface groups obtained by common photometric assays. We map thiol and amine groups introduced on silica NPs (SiNPs), titania stars (Ti), silica inverse opals (SiOps), and polystyrene NPs (PS NPs). We show that the method is suitable to map local, clustered inhomogeneities of the reactive sites on single SiNPs introduced by masking certain areas during surface functionalization. Mapping precise positions of reactive surface groups is essential for the design and the tailored ligation of multifunctional nanomaterials.

INTRODUCTION

The surface functionalization of nanoparticles (NPs) with specific functional groups and small molecules is an extremely important first step for most applications of nanoparticles in nanomedicine, drug delivery and catalysis. The initial surface functionalization is used to introduce reactive groups to stabilize the NPs, to influence compatibility between various NPs[1-3] and proteins[4-7] and importantly, as reactive sites to conjugate various further molecules like antibodies,[8] enzymes, therapeutic agents[9] and polymers.[10-13] Depending on the substrate particle, a wide variety of molecules and ligands are used for the introduction of the reactive groups.[14] Organofunctional alkoxysilanes such as aminosilanes[15-16] and mercaptosilanes[17] generate respectively terminal amino and thiol groups on most metal oxide nanomaterials, thiolated ligands are used for gold surfaces, *etc*. The amino and thiol groups are among the most important and most used for selective labelling and conjugation sites on nanomaterials.[18] Next to the quantity, it is essential where these initially introduced functional groups are generated locally on a single nanoparticle. Their position is essential for all further conjugation steps and also overall particle properties[19] and is often influenced by the functionalization reaction, the intrinsic binding and condensation sites for these molecules which vary, *e.g.*, with different crystal facets on the substrate NP[20] or on by-design patterned and patchy particles.[21]

New methods enable the mapping of receptor recognition motifs derived from ligated and adsorbed biomolecules on the surface of nanoparticles[22-23] and this potentially allows the microscopic molecular organization to be connected to biological impacts, receptor recognition and other key outcomes. When the initial reactive sites during a biomolecular conjugation are neglected, due to the absence of advanced methodologies,[8] these particles

will not present the intended interaction and will fail to manifest the desired biological identity.[24] Our recent explorations indeed suggest that many conjugated or functionalized particles that have been used *in vitro* and *in vivo* over the past decade may fall within that category. Indeed, in the presence of biological media this effect may be further amplified,[23] possibly explaining previous complex biological outcomes.[7] These difficulties may be so significant as to materially affect judgements on the potential future value of nanomedicine targeting, possibly confounding (fixable) technical aspects (such as control of ligation), with long term strategic difficulties in the delivery of the nanomedicine project.

The determination of the local position of the functional and reactive groups is often challenging other than their quantification performed, *e.g.*, via photometric assays. When electron microscopy is applied to characterize the local structures of nanomaterials, however, small organic molecules or functional groups can normally not be visualized with sufficient contrast. Therefore specific labelling is required. Electron dense gold NPs (AuNPs) have been adopted as a marker due to its inert nature and amplitude and phase contrast in electron microscopy,[25] hence enabling an easy distinguishability from less electron dense substrate materials and thereby enhancing the image processing. This is employed in immunolabelling where antibody-modified AuNPs (usually 5 to 15 nm) label specific epitopes on cells, cell compartments, or in the protein corona of nanoparticles.[22, 26-28] Smaller gold nanoclusters (AuNCs) have been widely used for site specific labelling of protein,[22, 24, 29] viral surfaces[30] *etc*., but have seldom been transferred to nanoscience, *e.g.*, functional groups on nanoparticles.[31] Au55 clusters are cuboctahedral particles with diameter of 1.4 nm and Au11 clusters have 0.8 nm diameter and label sites down to a resolution of 15 angstrom.[32]

Herein, we investigate AuNCs for mapping reactive thiol and amine groups on individual silica nanoparticles (SiNPs). SiNPs where chosen due to their versatility as substrate for surface functionalization, platform for drug delivery,[33] catalysis, fundamental bionanoscience[18] and the difference in electron density from Au to obtain sufficient contrast.[34] We adjusted the number of reactive groups on the particles, quantified them by photometric assays and subsequently mapped distribution of AuNCs by measuring the distances between single AuNCs on labelled SiNPs and by evaluating unspecific AuNCs binding. The technique was transferred to a variety of other nanomaterials such as SiOps, PS NPs and Ti stars. Further, we created patterns of thiol groups on SiNPs by a) *in situ* thiolation of breaking sintering necks in a colloidal crystal of SiNP creating clusters of thiol groups in the fusion zone and b) by adsorbing zinc oxide (ZnO) or iron oxide (IO) NPs as a "mask" on SiNPs surface during thiolation which were later selectively removed to form clustered thiol groups and finally mapped with AuNCs to recognize the patterns. The presented techniques provide an essential basis for the sub – 2 nm precise mapping of reactive sites on single nanoparticle to detect and advance the tailored placement of functional ligands for nanoscale positioning of the functionality on designed nanomaterials.

RESULTS AND DISCUSSIONS

Thiolation and amination of SiNPs.

In the first step, we introduced thiol and amine groups on SiNPs using (3-mercaptopropyl)trimethoxysilane (MPTMS) and (3-aminopropyl)triethoxysilane (APTES) respectively, in controlled surface density by varying the ratios of SiNPs (89 ± 3 nm) and the silane precursors in an initial functionalization step. Using photometric assays namely

Ellman's (5,5'-dithiobis-(2-nitrobenzoic acid)-based) assay for thiols and ninhydrin assay for amines, the resulting surface density of thiols was determined as 0, 0.02, 0.10, 0.30, 0.81, and 1.99 SH/nm^2 (Figure S1). For the aminated SiNPs, the surface amine densities were 0, 0.80, 1.36 and 4.42 NH_2/nm^2 (Figure S1). These measured concentrations represent fractions of a monolayer of silane molecules on the 89 ± 3 nm SiNPs which is theoretically ~5 per nm² considering that a silane molecule occupies a cross section of 0.2 nm^2.[35-36] Further particle characterizations (particle size distributions measured by differential centrifugal sedimentation (DCS) and dynamic light scattering (DLS)) are given in Figure S2 and S3.

AuNC-based reactive group mapping.

The principle of the AuNCs-based mapping of the distributions of thiol and amine groups is illustrated in Figure 1A. We employed commercially available 1.4 nm AuNCs with either monomaleimide groups (Mal – AuNCs) to detect thiols or mono-sulfo-N-hydroxysuccinimide ester groups (NHS – AuNCs) for specific detection of amines (Figure 1B and C). A key factor that determines the resolution of the mapping of the functional groups by AuNCs is the size of the AuNCs. For example, a 1.4 nm AuNCs has a cross sectional area of 1.54 nm^2. A silane group occupies a surface area of approximately 0.2 nm^2,[35-36] which implies that each AuNCs can occupy a maximum of 5 to 7 silane molecules in case of a fully covered surface (~5 groups per nm² correspond to a silane monolayer calculated from the silane cross section), thus determining the theoretical upper limit of detection for a single AuNC (Figure 1D). However, if the surface density of functional groups is lower than about 0.65 groups per nm^2, one AuNC is theoretically capable to detect a single functional group as only one functional group is available on the cross section of an AuNC. Smaller AuNCs, for example 0.8 nm AuNCs would lower the upper detection limit

per single AuNC to 2 to 3 functional groups per nm^2 at maximum surface density, however, provide less contrast in conventional TEM imaging, thus decreasing the overall detectability (see Figure S4 for measurements with 0.8 nm AuNCs). The technique is generally restricted to the material contrast of AuNC and the substrate particle during TEM imaging. This depends on the resolution of the available equipment, the substrate particle material and the size of the AuNCs and cannot easily be generalized but adapted, *e.g.*, by varying the size of the AuNCs. In our scenario, we found that 1.4 nm AuNCs could still be observed on 200 nm SiNPs particles and different other materials of various sizes (see below), while lowering SiNPs particles size resulted in increased contrast and detectability due to less silica interacting with the electron beam.

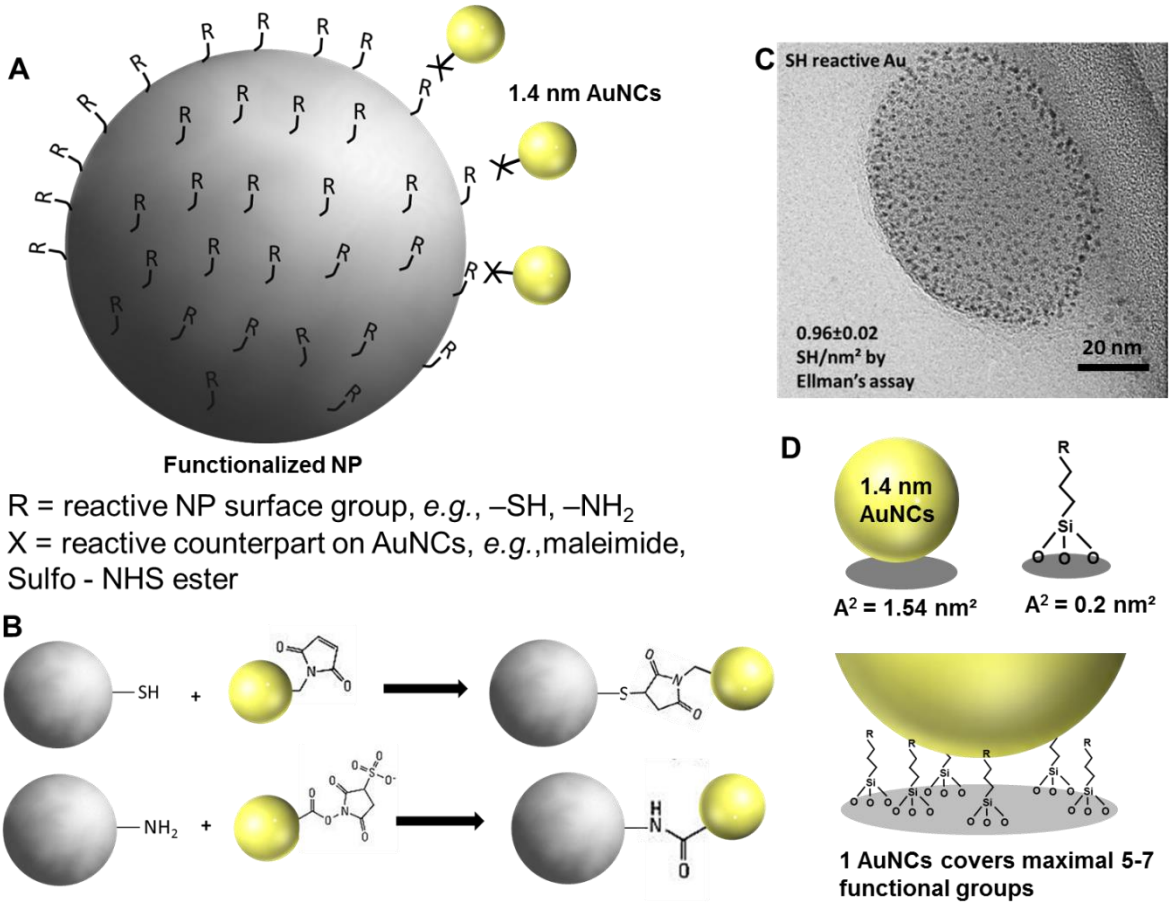

Figure 1: (A) Illustration of a NP functionalized with reactive groups such as thiol or amine groups. The AuNCs react specifically via maleimide or NHS ester functionality with the thiol and amine groups, respectively. (B) Reaction mechanism scheme representing reaction of thiol with Mal – AuNCs (top panel) and amines with NHS – AuNCs (bottom panel). (C) TEM image of thiolated SiNPs (0.96 ± 0.02 SH/nm^2) after reaction with Mal – AuNCs. The black dots correspond to AuNCs bound to the thiol groups on the NPs. (D) A silane molecule occupies a cross sectional area of 0.2 nm^2 while 1.4 nm AuNCs occupies an area of about 1.54 nm^2, thus proposing that 1 AuNC can cover maximal 5 – 7 functional groups, depending on the surface density of the functional group.

Characterization of AuNCs.

The AuNCs were primarily characterized in detail to determine their size distribution, contrast over SiNPs in TEM and their reactivity. TEM and gel electrophoresis analysis confirmed the monodispersity of the AuNCs (Figure S5). A negligible contamination with larger AuNPs of a size of about 5 nm was detected in a frequency of about one 5 nm AuNPs per one thousand 1.4 nm AuNCs (Figure S6). We examined the contrast of AuNCs in TEM by drop casting first a layer of AuNCs and then a layer of 80 nm SiNPs on top confirming

that the AuNCs are completely visible in transmission mode with SiNPs background (Figure S7). In terms of the selectivity of the maleimide function towards thiol groups, a certain degree of cross-reactivity of the Au surface of Mal – AuNCs towards thiols on the SiNPs may be expected and has to be considered as a further potential binding mechanism of the AuNCs to the surface thiols. However, we suggest that the maleimide-thiol binding is sterically more likely than the Au-thiol binding as the Au surface is covered by maleimide groups. In addition, for the purpose of mapping immobilized thiol groups, a thiol-specific cross-reaction does not have a disadvantage as long as the binding occurs via thiol groups. Nevertheless, we investigated how many thiols can react with one AuNC when the thiols are mobile (Figure S8) resulting in about maximally 15 – 30 per AuNC. Considering also the cross section area of a 1.4 nm particle, a single AuNC occupies sterically maximal only 5 to 7 thiols which may then bind to the AuNC, see Figure 1 and the impact on the thiol mapping is considered negligible.

Characterization of AuNC-mapped SiNPs.

For observing the binding of AuNCs on functionalized SiNPs, an initial characterization was done by differential centrifugal sedimentation (DCS) analysis in a sucrose density gradient, where the size distribution analysis by DCS is sensitive towards variations in the NPs overall sedimentation properties and thus to binding of denser AuNCs onto the less dense SiNPs.[22] SiNPs functionalized with different thiol and amine surface densities were reacted with AuNCs and analyzed. Figure 2A (right) show the peak of apparent diameter after thiol mapping which was extracted from size distributions as shown in Figure 2A (left) and in Figure S2. Similar measurements have been performed using aminated SiNPs and NHS – AuNCs, respectively (Figure 2B and S3). After reaction with

AuNCs, a shifted apparent diameter can be observed. The higher the surface density of functional groups (either thiols or amines), the more AuNCs bind to the SiNPs thus increasing the overall particle sedimentation properties resulting in greater size shifts in the DCS analysis. This suggests a strong correlation between the photometrically determined functional group densities and the measured size shifts. We thus simulated the apparent diameter as a function of AuNCs loading on SiNPs and compared it with the AuNCs binding as function of the surface density of reactive groups (Figure 2C). The measured shifts and slopes correspond to the simulations representing an increasingly establishing AuNC layer; the more reactive groups are exposed at the SiNPs as expected from number of surface groups determined by photometric assays.

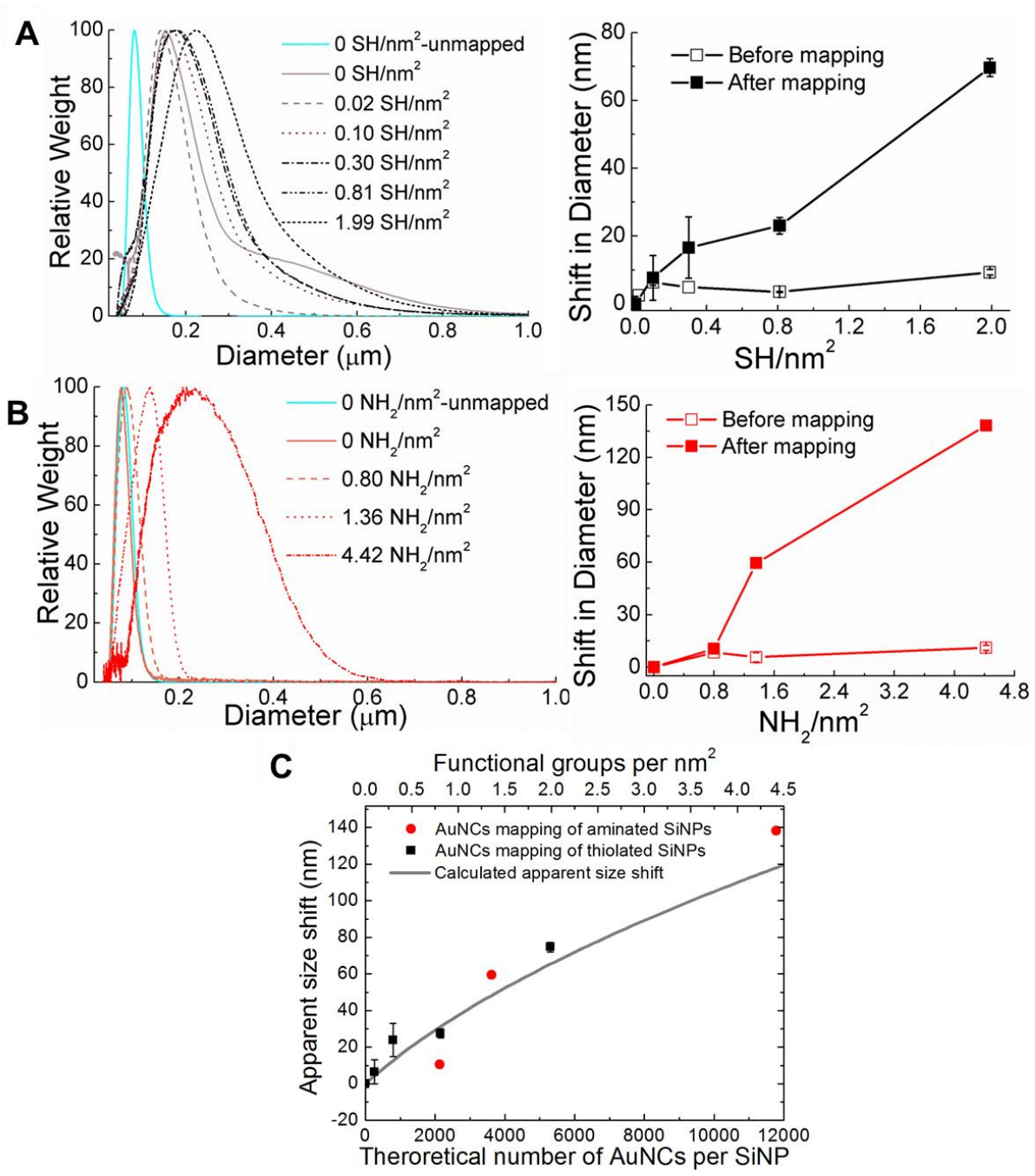

Figure 2: DCS analysis after AuNC-mapping of thiolated (A) and aminated (B) SiNPs, respectively. The size distribution showing the apparent diameter (left panel) shifts as function of reactive group surface density due to altered sedimentation properties. The right panel shows the extracted and plotted peaks of the apparent diameter before and after mapping with AuNCs versus the photometrically determined functional group densities (right panel). The error bars represent the standard deviations from 3 independent measurements, lines on right panels are guides to the eyes. (C) Simulations of the apparent diameter as a function of the number of AuNCs on SiNPs and compared with the surface densities of reactive functional groups and measurements shown in A and B.

The distribution of the functional groups on the SiNPs' surface after mapping was visualized using transmission electron microscopy (TEM). The TEM images in Figure 3A, B and S9 shows a homogeneous distribution of AuNCs bound to the thiols and amines, respectively on the SiNPs surface which could be expected from a homogeneous silanization of the surface. It is observed that as the concentration of functional groups on the surface increases, a higher surface density of AuNCs on the SiNPs is detected reflecting the higher concentration reactive sites. We found that the non – thiolated bare SiNPs (0 SH/nm^2) which have been mapped as a reference, also contain several AuNCs bound (Figure 3A), attributed to a certain amount of non-specific binding events of the Mal – AuNCs to the SiNPs' surface. However, there is almost no unspecific binding of NHS – AuNCs to bare SiNPs observed. This can be due to the strong negatively charged sulfonate group on the NHS – AuNCs, which is considered responsible for reducing the non-specific binding to the negatively charged bare SiNPs under experimental conditions. For aminated SiNPs, which expose positive surface charges from protonated amines, the sulfonate groups facilitate the conjugation reaction.

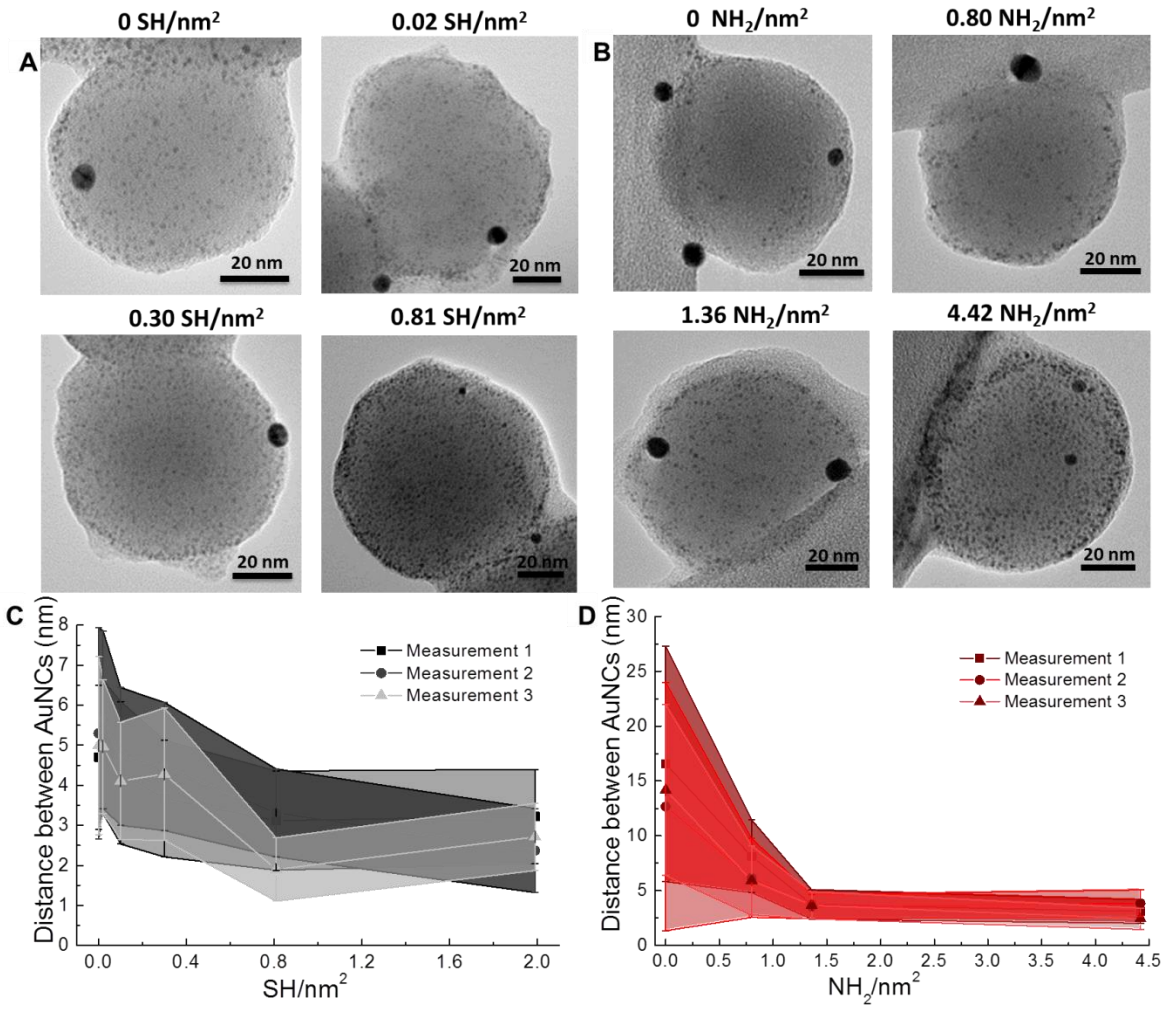

Figure 3: Representative TEM images of single AuNC-mapped SiNPs bearing different surface densities of reactive thiol (A) or amine (B) groups, the scale bar is 20 nm. (C) and (D) show measurements of the distance between AuNCs on the surface of three single SiNPs – SH and SiNPs – NH_2, respectively as function of the functional group surface density. Further details on the procedure are given in Figure S10. C and D were obtained from at least 1500 and 1200, respectively distance measurements and each data point represents the average and standard deviation of at least 100 distance measurements. The shaded areas represent the standard deviation between distances measured on single particles and measurement 1-3 represents the result for three individual particles. The decreasing distance at higher functional group density represents the increasing surface packing with reactive sites.

The surface density of the AuNCs can be determined by measuring the surface distance between the AuNCs on the TEM images to correlate it with the numbers of thiol and amine groups obtained from photometric assays. For the differently functionalized and AuNC-mapped SiNPs, a circular region with a diameter of 60 – 70 nm was selected such that the edge of the SiNPs was avoided and a maximum of 10 nm distance was kept from the periphery of the SiNPs where the projection error is largest (Figure S10). The same procedure

was used in recent theoretical study by Besser *et al.*[37] Figure 3C and D show measurements of three individually mapped SiNPs and applying a minimum of 100 distance measurements per object. The distance measurements and standard deviations verify that as the concentration of the functional groups increases, the distance between each AuNCs decreases from approx. 5 ± 0.3 nm to 2.8 ± 0.4 nm for thiolated SiNPs and from approx. 14.5 ± 2 nm to 3.1 ± 0.7 nm for aminated SiNPs, corresponding to the relative distance between the reactive functional groups and hence confirming the increasing surface density of the functional groups on SiNPs. A similar dependency of functional group distances was also reported in the theoretical study of Besser *et al*. when considering random arrangement of the functional groups.[37] The shaded region in the Figure 3C and D represents the standard deviation between distances measured on a single particle. The maximal deviation narrows down from about 4.5 to 2.0 nm for thiolated SiNPs and from 25.7 to 2.2 nm for aminated SiNPs on average indicating the decreasing distance of AuNCs. By TEM analysis, it is experimentally simpler to acquire images from which only the coordinates of the AuNCs from the whole surface of the SiNPs projected onto a plane. We showed before that pairwise distances vary slightly from geodesic distance of randomly distributed smaller particles on a sphere.[22] However, our models suggested that the effects in the distance distributions that arise from projections instead of geodesic distances are negligible compared to the influence of the distributions of reactive surface sites on the measured AuNCs distances. Thus, we use the value here rather as an approximation that represents the average density of the surface distribution of the AuNCs rather than true geodesic distances between single functional groups.[22] By different tilting of the SiNPs during the imaging in the TEM and thus acquiring different orientations one could generate a full map of the reactive sites if a more detailed analysis is necessary.

Mapping local assemblies and patches of reactive groups.

The aim of this study is to introduce a method to map single reactive group on single nanoparticle in a sub – 2 nm resolution to obtain an understanding of the position and distribution of such groups on nanomaterials. The AuNC-mapping (Figure 2) suggests that thiol and amine groups are homogeneously distributed on the SiNPs surface after functionalization. To test if inhomogeneous functionalization can be identified by AuNC-mapping, we applied two methods to disturb the homogeneous functionalization and generate clustering of functional groups on the SiNPs. As a first method, we created sintering necks between adjoining SiNPs in a colloidal crystal of 200 nm SiNPs (SiNPCC) by heat treatment, subsequently, the remaining free silanol groups were blocked by esterification with an alkane. Then the sintering necks were cracked by sonication and the newly created free particle surface was simultaneously functionalized using MPTMS to generate thiol groups. The process is schematized in Figure 4A and S11. After AuNCs mapping of thiolated and non – thiolated particles, we observed clustering of AuNCs in areas which correspond to the sintering necks, however these clusters were not observed on non – thiolated SiNPCC, while a slight non-specific adsorption was observed homogeneously distributed over the particle surface. The adhesion of the AuNCs seems to be pronounced at the edges of the patches. We suggest that this is due to a preferential functionalization of the patch-edges with the silanes as our controls with non-silanized particles did not indicate AuNC assembly in patches and at edges. Instead, a clearly distinguishable random non-specific interaction is seen on non-silanized samples confirming that cracked sintering necks were preferentially functionalized by MPTMS and that AuNCs detect such inhomogeneities (Figure 4B).

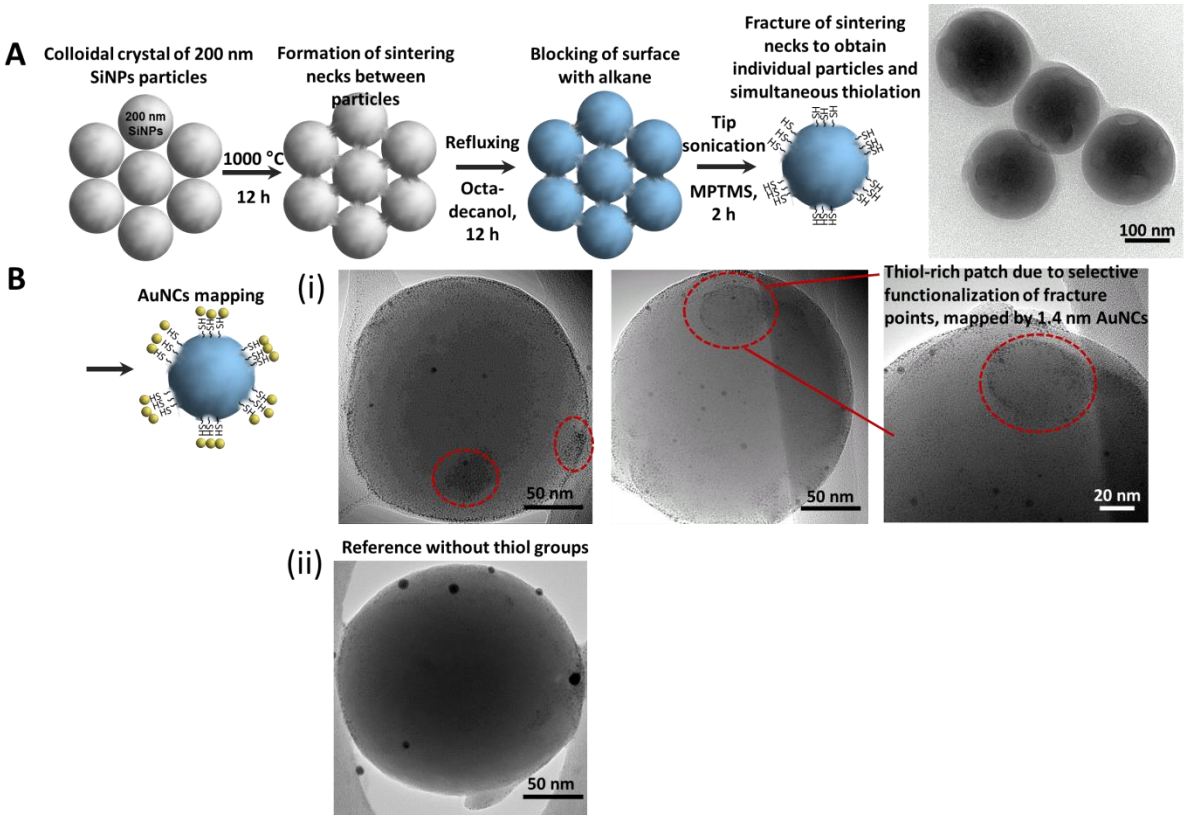

Figure 4: (A) Schematic illustrating the sintering process of SiNPs to obtain SiNPCC. (B) Mal – AuNCs mapping of SiNPCC, (i) obtained by thiolation while breaking of sintering necks to obtain thiol-rich surface patches at the fracture points detected by the AuNCs mapping and (ii) reference SiNPCC synthesized without thiolation while breaking sintering necks after AuNCs mapping.

As a second method, similar to a lithographic approach, adsorbing small, aminated and positively charged 5 nm Zinc oxide (ZnO) or 10 nm iron oxide (IO) NPs on the negatively charged SiNPs before functionalization as a "mask" before MPTMS addition (approximately 30 ZnO or IO NPs were added per SiNPs and any non – adsorbed masking particles were removed by washing). After subsequent functionalization, the ZnO or IO NPs template was selectively dissolved and surface thiol groups were AuNCs – mapped. The adsorbing ZnO and IO NPs may have two effects during functionalization of SiNPs. First, either ZnO or IO NPs block some of the SiNP surface area. Nevertheless, the silane precursors are expected to diffuse also into gaps between the blocking and substrate particles. Second, and assumingly more significant, as the silanes also bind onto hydroxyl groups

present on the surface of ZnO or IO NPs, these particles may deplete the precursor available for coating the SiNPs' surface. Thus, we expect to observe gaps in the AuNC-reactive site map which potentially due to combination of blocking surface area and a depletion mechanism. Considering the complexity of the process during reaction in a multicomponent colloidal system, we may not expect that the measured map necessarily exactly reproduces the template obtained of ZnO and IO adsorbing on SiNPs, however we can prove potential of the AuNC-mapping to detect any disturbance in the homogeneity of the reactive site distributions. Figure 5A illustrates the process and Figure 5B shows the results.

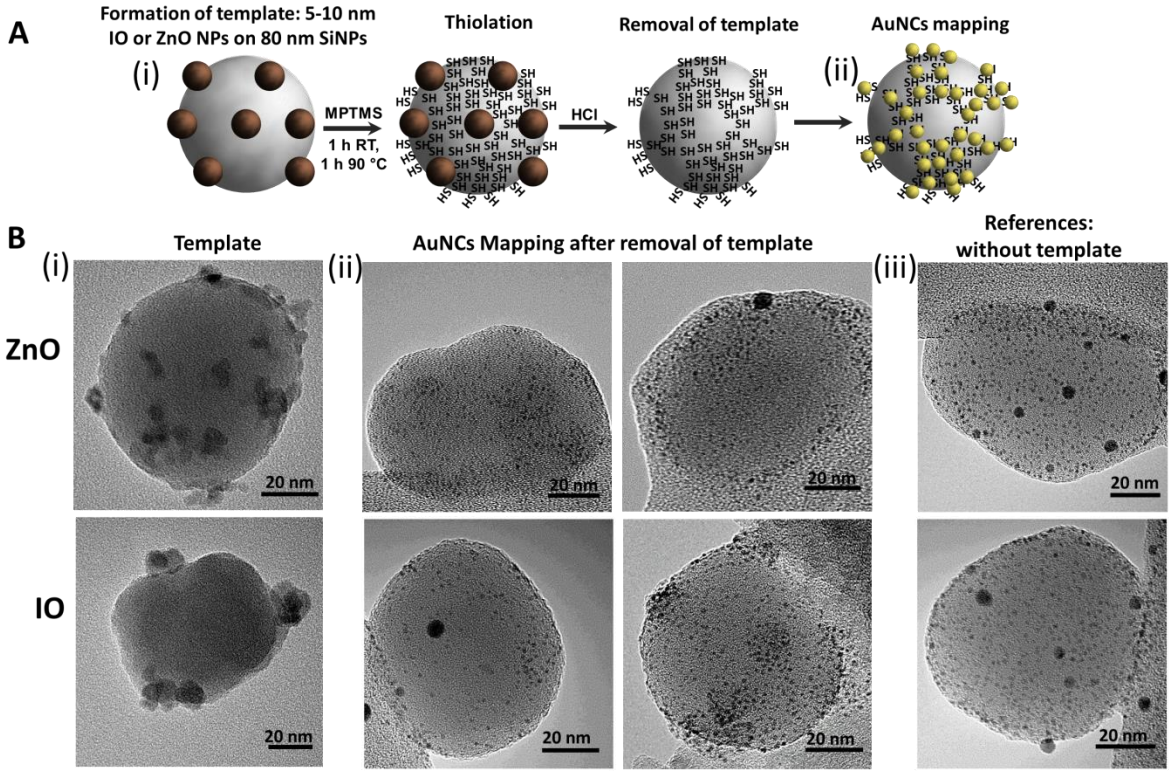

Figure 5: (A) Illustration of the procedure to block SiNPs with ZnO and IO NPs during thiolation which were subsequently mapped with Mal – AuNCs. (B) TEM images of Mal – AuNCs mapped SiNPs where (i) shows the template (ZnO and IO NPs adsorbed on SiNPs) (ii) TEM images after thiolation, removal of template, and AuNCs mapping. A more heterogeneous distribution of AuNCs was observed as compared to (iii) reference SiNPs which underwent the same functionalization steps but without ZnO and IO templates. Here, a homogeneous distribution of reactive thiol groups and AuNCs are observed proving that AuNCs mapping can identify inhomogeneous reactive site distributions on single nanoparticles.

When the ZnO or IO NPs were adsorbed during functionalization, it can be noticed that the amount of AuNCs mapped thiol groups on the surface decreased and spaces occur which can be attributed to the effect of ZnO and IO NPs that were present on the SiNPs during functionalization (Figure 5B i and ii). We followed the process using the Ellman's assay to obtain an ensemble measure of the number of thiol groups (Figure S12) and it confirms that the removal of ZnO and IO NPs decreases the overall number of reactive thiols. Figure 5B (iii) shows the reference thiolated SiNPs where the surface has not been blocked with ZnO or IO NPs and when mapped, it can be observed that surface is homogeneously covered with thiol groups. These reference SiNPs were treated in the same manner as the SiNPs blocked with ZnO and IO NPs to examine if the treatment with 0.06 M HCl and 3 M HCl used to selectively dissolve the blocking ZnO and IO NPs, respectively, can affect the thiol groups. No significant influence can be observed before and after acid treatment on the thiol functional groups functionalized without ZnO or IO NPs templates. As mentioned above, the inhomogeneity generated by the template NPs can be created by different mechanisms: A direct blocking of the SiNPs surface is rather unlikely considering that the small MPTMS molecules would diffuse in the gaps between an adsorbing masking ZnO and IO NPs and the SiNPs surface whose contact area is indefinitely small considering their spherical nature. However, the ZnO and IO NPs may react with MPTMS and so deplete MPTMS for reaction with the surface of the SiNPs, disturbing the functionalization homogeneity while no clear pattern can be observed and may also not be expected from the random assembly of the templates. The hypothesis is supported by the fact that only a certain amount of MPTMS corresponding to a half monolayer calculated for the bare SiNPs was used in the functionalization process and available precursors are limited. Nevertheless, further influences by dissolution conditions and dissolution products of the ZnO and IO NPs

on the thiol reactivity cannot be entirely excluded by TEM analysis which is by definition restricted to limited analysis areas and single particles in high resolution. For an extensive and direct quantitation and statistical analysis of a representative set of AuNCs maps per SiNP sample, in future an automated image acquirement and analysis solution is necessary and we are working on this.

Mapping of other materials.

To establish if the concept of the AuNCs mapping can be transferred to other materials, different functionalized nanostructures namely silica-based inverse opals (SiOps), polystyrene (PS) NPs and titania stars (Ti) were investigated after thiolation or amination and respective AuNC-mapping, confirming the procedure is not restricted to silica (Figure 6).

For bare SiOps (Figure 6A) there is a significant non – specific binding of the Mal – AuNCs more pronounced than before seen for SiNPs. This is possibly due to a potential porous nature of the structure and did not allow to distinguish the presence of thiols on the surface by AuNC-mapping. Nevertheless, the non-specific AuNCs binding is substrate dependent and needs to be considered separately for each material type and structure and the type of AuNC used as shown above.

Also commercially available PS NPs were used for investigating the AuNC-mapping of surface amines. From Figure 6B, it can be observed that also the PS NPs show a certain extend of unspecific binding of the NHS – AuNCs which was not observed for SiNPs. Although amines could be detected on PS – NH_2 but not on PS NPs by the ninhydrin assay on these particles (data not shown), they could not clearly be represented by AuNC mapping. The reason for this remains unclear perhaps due to the complex unknown surface structure and chemistry of PS – NH_2 influencing the binding. Nevertheless, the density contrast of the

AuNCs on the PS particles enables the observation of the AuNCs and proved PS to be a further suitable mapping substrate.

Ti stars synthesized as presented by Li *et al.*[31] (Figure 6C, D and E), and later functionalized using APTES to obtain an aminated surface. Figure 6D and E, represents bare Ti stars before and after mapping with NHS – AuNCs respectively. The bare and aminated Ti NPs were mapped using NHS – AuNCs and from Figure 6C, it can be observed that for the non-functionalized NPs (top panel of the Figure 6C) a small and negligible amount of AuNCs unspecifically bind to the stars' surface. However, for the amine functionalized Ti stars (lower panel of the Figure 6C), the binding of the AuNCs can be clearly observed and amine groups on the surface of the Ti stars could be identified. The right side of Figure 6C represents the zoomed images of the Ti stars' surface and the difference between non-functionalized and functionalized surfaces can be observed. Mapping the Ti surface, nevertheless high magnifications were necessary to observe the AuNCs against the TiO_2 background.

From the above examples of different materials being mapped with AuNCs, it has been clearly displayed that the mapping method is not restricted to one material type but material contrast and non-specific binding need to be considered for each material. More detailed and elaborate elemental mapping and scanning TEM analysis may be suitable to increase the material contrast while reaction conditions (solvent, pH, surfactants, washing steps *etc*.) may be explored in future for reducing non-specific binding, in addition to an automation of image acquirement and analysis.

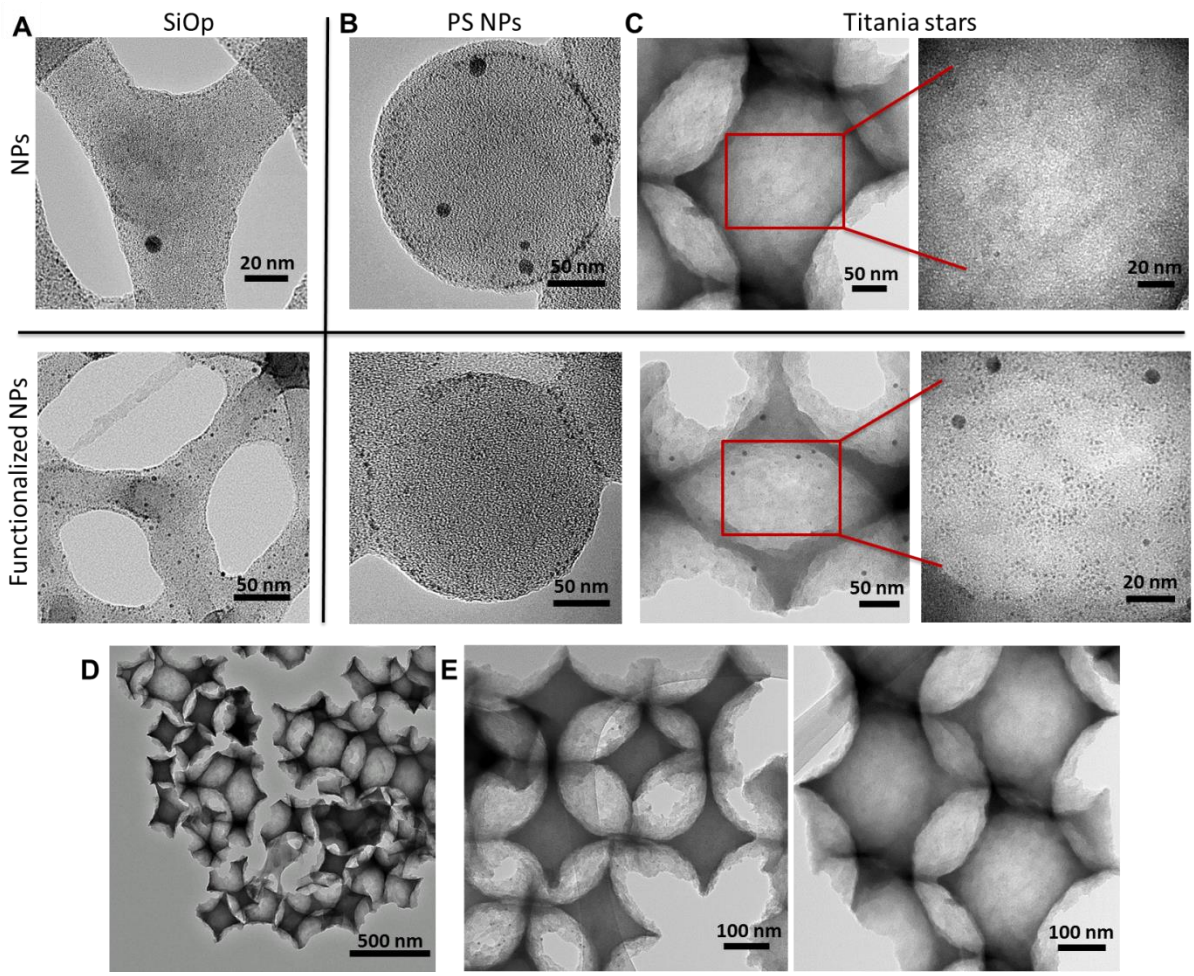

Figure 6: Transferring the AuNC mapping to various nanomaterials. (A) Silica inverse opals, SiOps (unfunctionalized, top panel and thiolated, lower panel) reacted with Mal – AuNCs . (B) and (C) PS NPs and titania stars, respectively that were reacted with NHS – AuNCs. Top panel, unfunctionalized, lower panel aminated nanomaterials. On the right of (C) zoomed in, higher magnification images of the titania stars are shown. (D) and (E) show overview images of unfunctionalized Ti stars before (D) and after (E) mapping.

CONCLUSIONS

We believe that a major effort is required to exert much more detailed microscopic control of the organization of ligated nanoparticles surface, and that tools to promote this will be of great value. Therefore, we introduce a concept of identifying spatial location, density and arrangement of reactive functional groups on the surface of single NP in the sub – 2 nm scale resolution. We map reactive thiol and amine surface functionalization of ~90 nm SiNPs of varying density using commercially available maleimide- and Sulfo-NHS- modified 1.4

nm AuNCs. The AuNCs binding were observed by DCS, sedimentation models and TEM to understand the distribution and surface distances of reactive functional groups per nm^2 on single SiNP and to correlate them with ensemble measurements of the functional groups by common photometric assays. We were able to transfer the method of mapping to different nanomaterials functionalized with either thiols or amines and identified patches and inhomogeneous distributions of functional groups. Depending on the surface functionality of the AuNCs and substrates, non-specific binding needs to be considered as well as material contrasts in TEM imaging. The method is an initial step towards analysis and control over molecular nanoscale precise placements of surface reactive sites for a tailored design of functional nanomaterials for many applications.

Materials and Methods

Materials:

APTMS ((3-aminopropyl)trimethoxysilane, 97%), APTES ((3-aminopropyl)triethoxysilane, 97%), Ethanol (99.5%), FITC (Fluorescein isothiocyanate isomer I, 98%), ThT (Thioflavin T), MPTMS ((3-Mercaptopropyl)trimethoxysilane, 95%), Ellman's reagent (5,5'-dithiobis-(2-nitrobenzoic acid) or DTNB), Ninhydrin (2,2-dihydroxyindane-1,3-dione), Potassium hydroxide, TEOS (tetraethyl orthosilicate, 99%), titanium(IV) butoxide (97%), Zinc acetate dihydrate (99%) were obtained from Sigma Aldrich. Monomaleimido AuNCs and Mono-sulfo-N-hydroxysuccinimide ester AuNCs were obtained from Nanoprobes. Polystyrene and aminated Polystyrene were obtained from Polysciences Inc. Water used in all the experiments were obtained from Milli-Q purification system (Millipore Corporation, Ireland).

Synthesis of SiNPs:

Fluorescent SiNPs were synthesized by co-condensation of tetraethylorthosilicate (TEOS) labelled with two dyes, namely Thioflavin T (ThT) and fluorescein isothiocyanate isomer I (FITC) as previously reported by Meder *et al.*[38] The core nanoparticles were further coated with a silica shell using TEOS, to prevent dye leakage and to provide more stability for the NPs. In brief, 0.91 g of ammonium hydroxide (26%) was added to 25 mL of ethanol (99.9%). Six mg of ThT was dissolved in 0.5 mL of ethanol and immediately added to the reaction. Then, 0.125 mL of solution prepared by mixing 2 mg of FITC, 1 mL of ethanol and 10 µL of APTMS (incubated in the dark for 4 h prior to addition) was added subsequently. The solution was stirred for 3 min followed by addition of 0.91 mL of TEOS and stirred overnight at 25 °C at 700 rpm. The nanoparticles were washed after centrifugation at 20,000 rcf for 25 min, the supernatant was removed and the pellet was redispersed in 25 mL ethanol by bath sonication. The procedure was repeated twice which was then followed by two more washing steps using 25 mL water and finally redispersed in water and the concentration was determined in mg per mL by measuring the dry weight in triplicates. Then the solution was heated to 90 ˚C and 1.2 µL of TEOS were added per mg SiNPs. After the reaction was left for 3 h at 90 ˚C at 700 rpm, the particles were washed three times with water by centrifugation at 20,000 rcf for 25 min and finally resuspended in water.

Thiolation of SiNPs:

Five mL of a 3 mg mL^{-1} suspension of SiNPs were mixed with 0.5 mL of a solution of MPTMS in ethanol. To vary the thiol surface density, the MPTMS concentration was adjusted to either 0, 0.02, 0.12, 0.25, 0.74 and 3.72 µmol, respectively per mg of SiNPs (these amounts correspond to 0, 0.1, 0.5, 1, 3 and 15 monolayer, respectively, considering square packing of circular areas with the cross section of the silane molecule of 0.2 nm^2 on the

SiNPs surface area considering spherical particles and the average diameter as determined by DLS).[36-37] The precursor solution was added to the SiNPs and was stirred for 1 h at 700 rpm and 25 ˚C followed by heating to 90 ˚C and subsequent stirring for another 1 h at 90 ˚C. After the reaction, the suspension was cooled down to room temperature and was washed three times by centrifugation at 20,000 rcf for 25 min and finally redispersed in water and stored in refrigerator at 4 ˚C.

Amination of SiNPs:

The same procedure as for the thiolation was followed replacing MPTMS by APTES. Varying concentration of amine density on the SiNPs' surface was obtained by adjusting the amount of APTES (0, 0.02, 0.25 and 0.74 μmol of APTES per mg of SiNPs according to 0, 0.1, 1 and 3 monolayer respectively).

Synthesis of thiolated SiNPCCs:

A suspension of monodisperse 200 nm SiNPs in water (approximately 20 mg mL^{-1}) synthesized as reported earlier[39] was centrifuged at 2000 rcf for 120 min. The supernatant was discarded and the opalescent pellet was dried at 70 ˚C for 48 h. The dried pellet was transferred to a furnace in an alumina dish and treated at 1000 ˚C for 12 h. Subsequently, the SiNP pellet was immersed in water for 24 h, then washed with ethanol and subsequently refluxed for 12 h in octadecanol to esterify the silanols with the corresponding alcohol.[40] The obtained particles are highly hydrophobic and not dispersible in water. The pellet was thus washed in ethanol and then immersed in a 1% solution of MPTMS in a 3:1 water:ethanol mixture, and tip sonicated for 2 h. The obtained particles were washed three times in water and resuspended by bath sonication. Larger particles were removed by a 1 min centrifugation at 1000 rcf and the supernatant collected for analysis.

Synthesis of aminated zinc oxide:

The synthesis of ZnO NPs was done as described by Zhao *et al*.[41] In a round bottom flask, 30 mL of 1.86 mmol of zinc acetate in ethanol was prepared and was refluxed for 90 min at 68 ˚C with stirring at 1500 rpm. After the refluxing, the solution was sonicated for 10 min and cooled down to room temperature (solution 1). In a glass vial, 15 mL of 4.11 mmol of potassium hydroxide in ethanol was prepared and was sonicated for 40 min at room temperature (solution 2). The solution 2 was added drop by drop to the above zinc acetate solution (solution 1), and was left stirring for 60 min at 1500 rpm at room temperature (solution 3). 15 mL of 0.34 mmol of APTES in ethanol was prepared and mixed with 1.5 mL water, which was added drop by drop to solution 3, with stirring at 1500 rpm and was left to react for 2 h. 10 mL of the aminated ZnO NPs was transferred to a dialysis membrane which was left in a water bath stirring at 200 rpm overnight. After the dialysis, the aminated ZnO NPs were stored in the fridge at 4 ºC. Before the experiments an aliquot was centrifuged at 20,000 rcf for 10 min to remove aggregates and the supernatant used for further experiments. The concentration of the ZnO NPs was obtained by measuring the dry weight of 1 mL of the suspension on an analytical balance and using particle volumes calculated from average diameters (TEM) and ZnO density of 5.61 g/mL. The number concentration of the ZnO NPs was determined by UV – Vis spectroscopy using the Beer – Lambert Law where the absorbance was measured using a cuvette with a path length of 1 cm. The extinction coefficient of ZnO NPs was determined earlier from a solution of ZnO NPs with known weight concentration. Therefore, the ZnO NPs suspension was serial diluted to 8 points and added to a 96 well UV – Vis multiwell plate and scanned for photometric measurement at 300 nm and fluorometric measurements at excitation at 340 nm and emission at 550 nm. All measurements were done in triplicates.

Synthesis of aminated iron oxide:

10 nm iron oxide NPs (IO, Fe_2O_3) were synthesized as described earlier[42-43] and functionalized with amine groups as done for SiNPs. Centrifugation steps were conducted for 10 min at 20000 rcf. The dry weight of 0.1 mL of the NPs was measured to determine the weight concentrations. The number concentration were calculated from the weight concentrations using particle volumes calculated from average diameter determined by TEM and an IO density of 5.24 g/mL. All measurements were done in triplicates.

Blocking SiNPs surface using ZnO and IO NPs:

Either the aminated ZnO or the aminated IO NPs (both positively charged) were adsorbed onto the negatively charged SiNPs in water at pH 7. Approximately 30 ZnO or IO NPs were added per SiNP (according to the number particle concentrations obtained as described above), to a suspension of 1 mg mL^{-1} SiNPs, which was left to react for 10 min with stirring at room temperature. After the reaction, the NPs-assemblies were spun down at 20,000 rcf for 7 min to remove any free ZnO or IO NPs and washed once with water and finally resuspended in water. 1 mL of the NPs-assemblies were kept for further characterization and rest of the SiNPs were used for thiolation. For thiolation, the NPs-assemblies were functionalized with 0.12 μmol of MPTMS per mg of SiNPs in 305 μL ethanol which was added per mg of SiNPs. The reaction was stirred at 700 rpm for 1 h at 25 ˚C followed by heating to 90 ˚C. After the reaction, the suspension was cooled down to room temperature and was washed three times by centrifugation at 20,000 rcf for 15 min and finally redispersed in water. After the washing step, another 1 mL was removed for further characterization. As a control, SiNPs were also thiolated under same conditions without addition of ZnO or IO NPs. After thiolation, the adsorbed ZnO or IO NPs on the SiNPs were

removed using hydrochloric acid (HCl). For removing ZnO, HCl was added to a final concentration of 0.06 M and immediately washed. The dissolution of the ZnO was also checked by the disappearance of photoluminescence of the particles under excitation by a UV lamp. The IO NPs were removed using 3 M HCl stirring at 700 rpm for 30 min. The SiNPs were centrifuged after the addition of the acid, at 20,000 rcf for 10 min. Subsequently the obtained SiNPs were washed and mapped with Mal – AuNCs. To comprehend the effect of the acid treatment on thiolated SiNPs, the reference without adsorbed ZnO or IO was treated with the above mentioned two concentrations of HCl and later mapped them with Mal – AuNCs. These nanoparticles were finally washed 4 times with water at 20,000 rcf for 10 min and finally redispersed in water. Ellman's assay and the AuNCs mapping were performed for the different fractions of the NPs collected over the various steps.

Synthesis of thiolated SiOps:

The synthesis procedure was adapted from Li *et al.,*[31] where the silica template structure was synthesized by templating with polymethyl methacrylate (PMMA) crystals that were synthesized by centrifugation of a suspension of 400 nm PMMA particles for 2 h at 1000 rcf. The supernatant was carefully removed and discarded. The opalescent pellet was dried for 1 week at room temperature. The PMMA colloidal crystal templates were half-immersed in a silica sol-gel precursor which contains 2 g of TEOS and 1 g of 1 M HCl. The precursor was further forced in to the interstices of the colloidal crystals by capillary forces and supported by applying a vacuum. The sol-gel colloidal crystal composites were stored at 70 ˚C for 24 h. The PMMA spheres were dissolved by repeated immersion in toluene and acetic acid and the silica template structure was harvested by filtration and finally dried in air. The obtained powder was dispersed in water and the surface was functionalized using MPTMS as explained above.

Synthesis of aminated titania stars:

Aminated titania stars (Ti) was synthesized by adapting the method of Li *et al*.[31] as described above. However, instead of immersion of the PMMA colloidal crystals in TEOS, we used 2 g of titanium (IV) butoxide in 1 g of 1 M HCl. After dissolution of the PMMA template in toluene and harvesting by filtration and air drying, 50 mg was added in 10 mL water and tip sonicated the mixture for 2 h to break the titania inverse opals into smaller titania stars. To remove larger particles and remaining unbroken inverse opals, the resulting solution was centrifuged at 1000 rcf for 1 min and harvested the supernatant containing smaller particles. These were subsequently washed 3 times in water by repeated centrifugation at 10000 rcf for 5 min. The titania stars were functionalized with amine groups as described above.

AuNC reaction with thiolated and aminated SiNPs:

To an aliquot of AuNCs, 0.4 mL of water was added such that the concentration of AuNCs is 15 nmol mL^{-1}. Four µL of the SiNPs (1 mg mL^{-1}) were added to 200 µL of water, followed by addition of 50 µL of AuNCs (which is approximately, $5x10^5$ AuNCs per ~90 nm SiNPs or about 50 monolayer) which was quickly vortexed for 20 sec. The reaction was left stirring at 700 rpm at room temperature for 2 h. The samples were washed four times with water by centrifugation at 20,000 rcf for 15 min and finally redispersed in 50 µL water.

Ellman's Assay:

The buffer required for the assay was composed of 0.5678 g of sodium phosphate dibasic (Na_2HPO_4), 14.9 mg of ethylenediaminetetraacetic acid (EDTA) and 40 mL of water and finally adjusted to pH 8. The Ellman's reagent solution (5,5'-dithiobis-(2-nitrobenzoic acid or DTNB) was prepared by dissolving 4 mg of DTNB in 1 mL of the buffer. As a

standard, MPTMS in ethanol was used and found linear in the range of 1500 to 1.5 µM. To 250 µL of the buffer, 5 µL of the Ellman's reagent was added followed by addition of 25 µL of the sample which was incubated at room temperature for 15 min. After the incubation, samples with nanoparticles were spun down using centrifugation at 20,000 rcf for 15 min to remove the particles and 200 µL of the supernatant was transferred to multiwell plate and the absorbance at 412 nm was measured using ThermoScientific Varioskan Flash Multimode reader. Each sample was done in triplicate, as controls unfunctionalized NPs and supernatants of functionalized NPs were analyze to determine background signal and exclude free thiols unbound to the NPs which was found negligible.

Ninhydrin assay:

For determining surface amino groups, 100 µL of the aminated NPs and reference NPs were resuspended into ethanol by centrifugation of the NPs at 20,000 rcf for 15 min followed by sonication in 1 mL of anhydrous ethanol. This step was repeated twice to reduce the concentration of water and NPs were finally redispersed in 0.5 mL anhydrous ethanol. 3.5 mg mL^{-1} fresh ninhydrin solution was prepared and 125 µL of the solution was added to the NPs, supernatants and standards. The reaction was left at 60 ˚C for 30 min where the colour changes from clear to blue – purple. After the reaction, the NPs were centrifuged at 20,000 rcf for 15 min and 200 µL of the supernatant was transferred to a multiwell plate and the absorbance at 566 nm was measured using ThermoScientific Varioskan Flash Multimode reader. Each sample was done in triplicates. For the calibration curve, APTES in ethanol was used and found linear in the range of 5000 to 78 µM by serial dilution; the same controls as described for the Ellman's assay were used.

Differential Centrifugal Sedimentation (DCS):

DCS was carried out using CPS disc centrifuge DC24000 (CPS Instruments Inc., U.K.) where 8 – 24 w/w % sucrose based gradient in water was used. All the measurements were carried out at 18,000 rpm. A calibration was done using poly (vinyl chloride) (PVC) standard (0.483 μm, Analytik Ltd., U.K.). Before each measurement, 0.1 mL calibration was injected followed by 0.1 mL of each sample using a calibrated Hamilton syringe (Hamilton GASTIGHT, Hamilton, U.K.) with an accuracy of ±1% within the injected volume.

Transmission Electron Microscopy (TEM):

TEM micrographs of the mapped NPs were obtained using FEI Tecnai G2 20 twin microscope (FEI, Inc., The Netherlands) at an accelerating voltage of 200 kV. The samples were prepared by drop casting 10 μL of the samples to a lacey formvar/carbon copper grid (300 mesh, Ted Pella, Inc., U.K.) which was then dried overnight. Further description of procedures from image analysis can be found in the supporting information.

ASSOCIATED CONTENT

AUTHOR INFORMATION

Corresponding Author

Correspondence should be addressed to Kenneth A. Dawson (kenneth.a.dawson@cbni.ucd.ie) or Fabian Meder (mederf@gmx.de).

Author Contributions

The manuscript was written through contributions of all authors. All authors have given approval to the final version of the manuscript.

ACKNOWLEDGMENT

S.T. would like to acknowledge the Irish Research Council (GOIPG/2013/104). F.M. acknowledges the support of the German Research Foundation (DFG), 'Forschungsstipendium' ME 4296/1-1. E.P. and K.A.D. acknowledge the Science Foundation Ireland (SFI, 12/IA/1422). The authors acknowledge the Imaging Core facility at the Conway Institute, UCD.

Supporting Information

Additional experimental details, photometric assay detection of number of functional groups, DCS and DLS measurements of thiolated and aminated SiNPs, contrast between 0.8 nm and 1.4 nm AuNCs in TEM, characterization of AuNCs to determine the monodispersity, comparison of larger AuNCs with majority of smaller AuNCs, TEM image of SiNPs on AuNCs, further characterization of Mal – AuNCs using reverse Ellman's assay, TEM image of AuNCs labelled thiolated SiNPs, distance measurement using TEM microscopy mapped images of thiolated and aminated SiNPs, reaction scheme of sintering steps with corresponding TEM images, Ellman's assay for surface blocking of SiNPs with ZnO and IO NPs. This material is available free of charge via the Internet at http://pubs.acs.org.

REFERENCES

1. Bernat, M.-S.; Judit, M.-F.; Patricia, G.-Q.; Nicolas, P.-P.; Hai-nan, X.; Neus, G. B.; Víctor, P.; Ramon, A. A.-P.; Luca, G., SERS efficiencies of micrometric polystyrene beads coated with gold and silver nanoparticles: the effect of nanoparticle size. *J. Opt.* **2015,** *17*, 114012.
2. Peiris, P. M.; Schmidt, E.; Calabrese, M.; Karathanasis, E., Assembly of Linear Nano-Chains from Iron Oxide Nanospheres with Asymmetric Surface Chemistry. *PLoS ONE* **2011,** *6*, e15927.
3. Pellegrino, T.; Manna, L.; Kudera, S.; Liedl, T.; Koktysh, D.; Rogach, A. L.; Keller, S.; Rädler, J.; Natile, G.; Parak, W. J., Hydrophobic Nanocrystals Coated with an Amphiphilic Polymer Shell: A General Route to Water Soluble Nanocrystals. *Nano Lett.* **2004,** *4*, 703-707.

4. Aubin-Tam, M.-E.; Hamad-Schifferli, K., Gold Nanoparticle−Cytochrome c Complexes: The Effect of Nanoparticle Ligand Charge on Protein Structure. *Langmuir* **2005,** *21*, 12080-12084.
5. Hristov, D. R.; Rocks, L.; Kelly, P. M.; Thomas, S. S.; Pitek, A. S.; Verderio, P.; Mahon, E.; Dawson, K. A., Tuning of nanoparticle biological functionality through controlled surface chemistry and characterisation at the bioconjugated nanoparticle surface. *Sci. Rep.* **2015,** *5*, 17040.
6. Lo Giudice, M. C.; Meder, F.; Polo, E.; Thomas, S. S.; Alnahdi, K.; Lara, S.; Dawson, K. A., Constructing bifunctional nanoparticles for dual targeting: improved grafting and surface recognition assessment of multiple ligand nanoparticles. *Nanoscale* **2016,** *8*, 16969-16975.
7. Salvati, A.; Pitek, A. S.; Monopoli, M. P.; Prapainop, K.; Bombelli, F. B.; Hristov, D. R.; Kelly, P. M.; Aberg, C.; Mahon, E.; Dawson, K. A., Transferrin-functionalized nanoparticles lose their targeting capabilities when a biomolecule corona adsorbs on the surface. *Nat. Nanotechnol.* **2013,** *8*, 137-143.
8. Kumar, S.; Aaron, J.; Sokolov, K., Directional conjugation of antibodies to nanoparticles for synthesis of multiplexed optical contrast agents with both delivery and targeting moieties. *Nat. Protoc.* **2008,** *3*, 314-320.
9. Wang, F.; Wang, Y.-C.; Dou, S.; Xiong, M.-H.; Sun, T.-M.; Wang, J., Doxorubicin-Tethered Responsive Gold Nanoparticles Facilitate Intracellular Drug Delivery for Overcoming Multidrug Resistance in Cancer Cells. *ACS Nano* **2011,** *5*, 3679-3692.
10. Dai, Q.; Walkey, C.; Chan, W. C. W., Polyethylene Glycol Backfilling Mitigates the Negative Impact of the Protein Corona on Nanoparticle Cell Targeting. *Angew. Chem., Int. Ed.* **2014,** *53*, 5093-5096.
11. He, Q.; Zhang, J.; Shi, J.; Zhu, Z.; Zhang, L.; Bu, W.; Guo, L.; Chen, Y., The effect of PEGylation of mesoporous silica nanoparticles on nonspecific binding of serum proteins and cellular responses. *Biomaterials* **2010,** *31*, 1085-1092.
12. Herda L. M.; Polo, E.; Kelly P. M.; Rocks, L.; Hudecz, D.; Dawson K. A., Designing the future of nanomedicine: current barriers to targeted brain therapeutics. *Eur. J. Nanomed.* **2014**, 6, 127.
13. Xie, J.; Xu, C.; Kohler, N.; Hou, Y.; Sun, S., Controlled PEGylation of Monodisperse Fe3O4 Nanoparticles for Reduced Non-Specific Uptake by Macrophage Cells. *Adv. Mater.* **2007,** *19*, 3163-3166.
14. Sperling, R. A.; Parak, W. J., Surface modification, functionalization and bioconjugation of colloidal inorganic nanoparticles. *Philos. Trans. R. Soc., A.* **2010,** *368*, 1333-1383.
15. Liu, Y.; Li, Y.; Li, X.-M.; He, T., Kinetics of (3-Aminopropyl)triethoxylsilane (APTES) Silanization of Superparamagnetic Iron Oxide Nanoparticles. *Langmuir* **2013,** *29*, 15275-15282.
16. Lu, H.-T., Synthesis and characterization of amino-functionalized silica nanoparticles. *Colloid J.* **2013,** *75*, 311-318.
17. Nakamura, T.; Yamada, Y.; Yano, K., Direct synthesis of monodispersed thiol-functionalized nanoporous silica spheres and their application to a colloidal crystal embedded with gold nanoparticles. *J. Mater. Chem.* **2007,** *17*, 3726-3732.
18. Izak-Nau, E.; Kenesei, K.; Murali, K.; Voetz, M.; Eiden, S.; Puntes, V. F.; Duschl, A.; Madarász, E., Interaction of differently functionalized fluorescent silica nanoparticles with neural stem- and tissue-type cells. *Nanotoxicology* **2014,** *8*, 138-148.

19. Colombo, M.; Fiandra, L.; Alessio, G.; Mazzucchelli, S.; Nebuloni, M.; De Palma, C.; Kantner, K.; Pelaz, B.; Rotem, R.; Corsi, F.; Parak, W. J.; Prosperi, D., Tumour homing and therapeutic effect of colloidal nanoparticles depend on the number of attached antibodies. *Nat. Commun.* **2016,** *7*, 13818.
20. Miclăuş, T.; Bochenkov, V. E.; Ogaki, R.; Howard, K. A.; Sutherland, D. S., Spatial Mapping and Quantification of Soft and Hard Protein Coronas at Silver Nanocubes. *Nano Lett.* **2014,** *14*, 2086-2093.
21. Huang, R.; Carney, R. P.; Ikuma, K.; Stellacci, F.; Lau, B. L. T., Effects of Surface Compositional and Structural Heterogeneity on Nanoparticle–Protein Interactions: Different Protein Configurations. *ACS Nano* **2014,** *8*, 5402-5412.
22. Kelly, P. M.; Åberg, C.; Polo, E.; O'Connell, A.; Cookman, J.; Fallon, J.; KrpetićŽeljka; Dawson, K. A., Mapping protein binding sites on the biomolecular corona of nanoparticles. *Nat. Nanotech.* **2015,** *10*, 472-479.
23. Lo Giudice, M. C.; Herda, L. M.; Polo, E.; Dawson, K. A., In situ characterization of nanoparticle biomolecular interactions in complex biological media by flow cytometry. *Nat. Commun.* **2016,** *7*, 13475.
24. Herda, L. M.; Hristov, D. R.; Lo Giudice, M. C.; Polo, E.; Dawson, K. A., Mapping of Molecular Structure of the Nanoscale Surface in Bionanoparticles. *J. Am. Chem. Soc.* **2017,** *139*, 111-114.
25. Alvarez, M. M.; Khoury, J. T.; Schaaff, T. G.; Shafigullin, M.; Vezmar, I.; Whetten, R. L., Critical sizes in the growth of Au clusters. *Chem. Phys. Lett.* **1997,** *266*, 91-98.
26. Hainfeld, J. F.; Furuya, F. R., A 1.4-nm gold cluster covalently attached to antibodies improves immunolabeling. *J. Histochem. Cytochem.* **1992,** *40*, 177-84.
27. Hainfeld, J. F.; Powell, R. D., New Frontiers in Gold Labeling. *J. Histochem. Cytochem.* **2000,** *48*, 471-480.
28. Lin, C.-A. J.; Yang, T.-Y.; Lee, C.-H.; Huang, S. H.; Sperling, R. A.; Zanella, M.; Li, J. K.; Shen, J.-L.; Wang, H.-H.; Yeh, H.-I.; Parak, W. J.; Chang, W. H., Synthesis, Characterization, and Bioconjugation of Fluorescent Gold Nanoclusters toward Biological Labeling Applications. *ACS Nano* **2009,** *3*, 395-401.
29. Aubin, M.-E.; Morales, D. G.; Hamad-Schifferli, K., Labeling Ribonuclease S with a 3 nm Au Nanoparticle by Two-Step Assembly. *Nano Lett.* **2005,** *5*, 519-522.
30. Marjomäki, V.; Lahtinen, T.; Martikainen, M.; Koivisto, J.; Malola, S.; Salorinne, K.; Pettersson, M.; Häkkinen, H., Site-specific targeting of enterovirus capsid by functionalized monodisperse gold nanoclusters. *Proc. Natl. Acad. Sci. U. S. A.* **2014,** *111*, 1277-1281.
31. Li, F.; Yoo, W. C.; Beernink, M. B.; Stein, A., Site-Specific Functionalization of Anisotropic Nanoparticles: From Colloidal Atoms to Colloidal Molecules. *J. Am. Chem. Soc.* **2009,** *131*, 18548-18555.
32. Bartlett, P. A.; Bauer, B.; Singer, S. J., Synthesis of water-soluble undecagold cluster compounds of potential importance in electron microscopic and other studies of biological systems. *J. Am. Chem. Soc.* **1978,** *100*, 5085-5089.
33. Malvindi, M. A.; Brunetti, V.; Vecchio, G.; Galeone, A.; Cingolani, R.; Pompa, P. P., SiO2 nanoparticles biocompatibility and their potential for gene delivery and silencing. *Nanoscale* **2012,** *4*, 486-495.
34. Argyo, C.; Weiss, V.; Bräuchle, C.; Bein, T., Multifunctional Mesoporous Silica Nanoparticles as a Universal Platform for Drug Delivery. *Chem. Mater.* **2014,** *26*, 435-451.
35. Barton, S. W.; Goudot, A.; Rondelez, F., X-ray structural study of polymerized octyldecyltrichlorosilane on water. *Langmuir* **1991,** *7*, 1029-1030.

36. Kojio, K.; Takahara, A.; Omote, K.; Kajiyama, T., Molecular Aggregation State of n-Octadecyltrichlorosilane Monolayers Prepared by the Langmuir and Chemisorption Methods. *Langmuir* **2000,** *16*, 3932-3936.
37. Besser, B.; Malik, S.; Baune, M.; Kroll, S.; Thöming, J.; Rezwan, K., The influence of the functional group density on gas flow and selectivity: Nanoscale interactions in alkyl-functionalized mesoporous membranes. *Microporous Mesoporous Mater.* **2017,** *237*, 38-48.
38. Meder, F.; Thomas, S. S.; Fitzpatrick, L. W.; Alahmari, A.; Wang, S.; Beirne, J. G.; Vaz, G.; Redmond, G.; Dawson, K. A., Labeling the Structural Integrity of Nanoparticles for Advanced In Situ Tracking in Bionanotechnology. *ACS Nano* **2016,** *10*, 4660-4671.
39. Hartlen, K. D.; Athanasopoulos, A. P. T.; Kitaev, V., Facile Preparation of Highly Monodisperse Small Silica Spheres (15 to >200 nm) Suitable for Colloidal Templating and Formation of Ordered Arrays. *Langmuir* **2008,** *24*, 1714-1720.
40. Van Helden, A. K.; Jansen, J. W.; Vrij, A., Preparation and characterization of spherical monodisperse silica dispersions in nonaqueous solvents. *J. Colloid Interface Sci.* **1981,** *81*, 354-368.
41. Zhao, L.-H.; Zhang, R.; Zhang, J.; Sun, S.-Q., Synthesis and characterization of biocompatible ZnO nanoparticles. *CrystEngComm* **2012,** *14*, 945-950.
42. Bee, A.; Massart, R.; Neveu, S., Synthesis of very fine maghemite particles. *J. Magn. Magn. Mater.* **1995,** *149*, 6-9.
43. Bollhorst, T.; Shahabi, S.; Wörz, K.; Petters, C.; Dringen, R.; Maas, M.; Rezwan, K., Bifunctional Submicron Colloidosomes Coassembled from Fluorescent and Superparamagnetic Nanoparticles. *Angew. Chem., Int. Ed.* **2015,** *54*, 118-123.

Insert Table of Contents Graphic and Synopsis Here

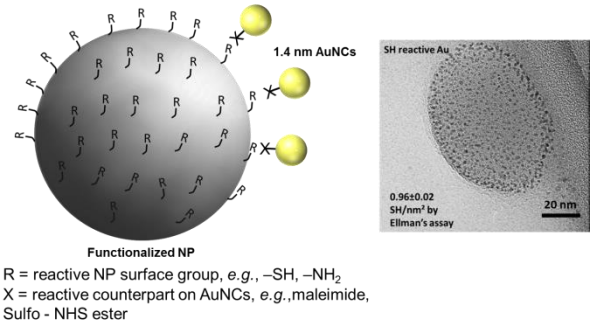

Supporting Information

Locating reactive groups on nanomaterials with gold nanoclusters – towards a surface reactive site map

Steffi S. Thomas, Matthew Coleman, Emma Carrol, Ester Polo, Fabian Meder, Kenneth A. Dawson**

Centre for BioNano Interactions, University College Dublin, School of Chemistry and Chemical Biology, Belfield 4, Dublin, Ireland.

Table of Contents

1 Additional experimental details

1.1 Modelling the apparent size shift in DCS due to AuNCs deposition on SiNPs

In DCS analysis, the sedimentation velocity is correlated with the density and the size of the particles based on a modified version of the Stokes equation that takes the g force into account acting on the particles and how this force varies with the radius of the centrifuge disc.

$$D = \sqrt{\frac{18\eta \ln(\frac{R_f}{R_i})}{(\rho_p - \rho_f)\omega^2 t}}$$

Where **D** is the particle diameter (cm), **η** is the fluid viscosity (poise), $\mathbf{R_i}$ and $\mathbf{R_f}$ are the initial and final radius of rotation, respectively (cm); $\boldsymbol{\rho_p}$ and $\boldsymbol{\rho_f}$ are the particle and fluid densities respectively (g/mL); **ω** is the rotational velocity (rad/s) and **t** is the time it takes the particle to travel from $\mathbf{R_i}$ to $\mathbf{R_f}$ (s).

In our case, AuNCs deposits on the surface of SiNPs resulting in an increased weight due to the higher density of Au compared to SiO_2 but only slight increases in the particle diameter. The overall particle density (SiNPs core + AuNCs) is complex and the apparent diameter is thus not directly related to the particle size but to the overall sedimentation properties. We thus used a general model to predict how the AuNCs deposition influences the apparent, measured particle diameter using the SiNPs size and density and AuNCs density as variables by the formulations below. Thereby, we consider the AuNCs deposition as a formation of a continuous Au layer with an equivalent number of AuNCs of diameter of 1.4 nm based on the following considerations. In the following, **r** is the diameter of the core SiNPs in nm, **s** is the

AuNCs layer thickness and AuNCs diameter, respectively in nm, $\boldsymbol{\rho_{SiNPs}}$ density of the SiNPs core (g/cm^3), $\boldsymbol{\rho_{AuNCs}}$ density of the AuNCs (g/cm^3), $\boldsymbol{\rho_{medium}}$ density of the medium, here for water it is 1 g/cm^3.

A solid 1.4 nm thick Au layer on SiNPs is equivalent to a certain number of AuNCs:

$$N_{AuNC} = \frac{4r^2}{3s^2}$$

A monolayer of AuNCs on a SiNPs is composed of fractions of this value depending on the packing of the AuNCs on the surface. *E.g.* for close cubic packing AuNCs, the monolayer consists of $\frac{\pi}{3\sqrt{2}}$ N_{AuNCs} per SiNPs.[1]

The volume of the core SiNPs is:

$$V_{core} = \frac{\pi r^3}{6}$$

The total (SiNPs core plus AuNCs coating) particle volume is:

$$V_{tot} = \frac{\pi(r+2s)^3}{6}$$

The AuNCs layer volume is:

$$V_{AuNC} = V_{tot} - V_{SiNP}$$

The net density:

$$\rho_{net} = \frac{V_{SiNP}\rho_{SiNP} + V_{AuNC}\rho_{AuNC}}{V_{tot}}$$

The relative sedimentation velocity (RSV) describes the rate at which molecules move in response to centrifugal force generated in a disc centrifuge. It is dependent on the particle density and relative sedimentation velocity of our particle system and thus can be obtained by

$$RSV = \frac{(\rho_{Net} - \rho_{medium}) \cdot (r + 2s)^2}{(\rho_{SiNP} - \rho_{medium}) \cdot (r + 2s)^2}$$

The apparent diameter is then given by:

$$D_A = r\sqrt{RSV}$$

1.2 Reverse Ellman's assay to determine the number of maleimide groups on Mal – AuNCs:

3 – Mercaptopropionic acid (3-MPA) was used for the preparation of a calibration curve, with an initial concentration of 1500 µM and dilutions thereof to obtain varying concentrations with final point being without any 3 - MPA.

For the sample preparation, to an aliquot of Mal – AuNCs (2 nmol), 37.5 µL of water was added, yielding a final concentration of 53.3 µM. From this initial concentration, 5 subsequent concentrations of 21.3, 10.7, 2.13, 0.43 and 0.09 µM were prepared in water. 10 µL of each AuNCs dilution was mixed with 10 µL of 3 – MPA (600 µM), which was reacted at room temperature for an hour with stirring at 600 rpm. To 250 µL of the Ellman's buffer, 5 µL of the Ellman's reagent was added followed by addition of 20 µL of the AuNCs with 3 – MPA and was left stirring to react for 15 min. The solutions were centrifuged using spin filter (3 kDa) to remove the AuNCs at 6797 rcf for 20 – 30 min. 150 µL of the filtered solution was collected and transferred to multiwell plate and the absorbance at 412 nm was

measured using ThermoScientific Varioskan Flash Multimode reader. Each sample was done in triplicates.

1.3 Gel – Electrophoresis:

A typical SDS gel was prepared using 4% acrylamide stacking gel and a 10% separation gel. Six nmol AuNCs were dispersed in 65 µL of 10 mM HEPES. Separately, 7 mL of running buffer and 3 mL of glycerol were mixed and 10 µL of this solution was mixed with 15 µL of the AuNCs. 20 µL of this mixture was added to the wells of the gel and as a molecular weight comparison, a protein ladder was used. A constant voltage of 150 V was applied for 45 mins across the gel to separate the differently sized AuNCs and to evaluate AuNCs' size distribution.

2 Supporting data

S1: Determination of funcitonal groups per nm^2 using photometric assays.

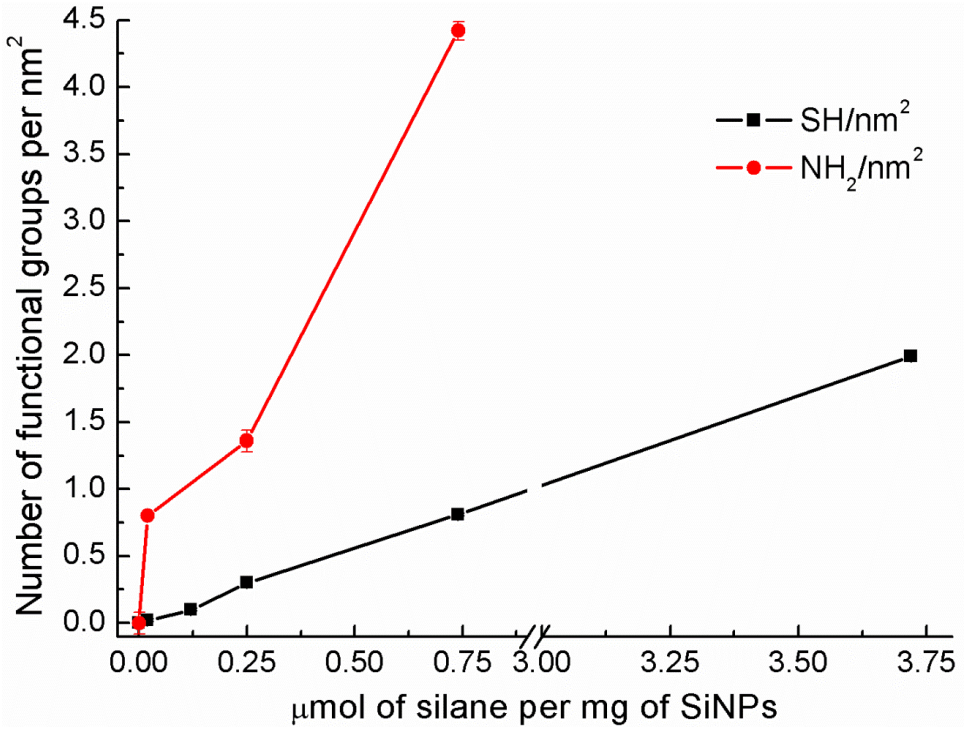

Figure S1: The number of functional groups per nm^2 measured using Ellman's photometric assay for the thiol group (black squares), where 6 various surface densities were investigated. While for the amine functional groups, the number of amine groups per nm^2 was determined for 4 different surface densities using Ninhydrin assay (red circles). The error bars represents the standard deviations from 3 individual measurements. Lines are guides to the eyes.

S2: Size measurement of thiolated SiNPs using (A) DCS and (B) DLS.

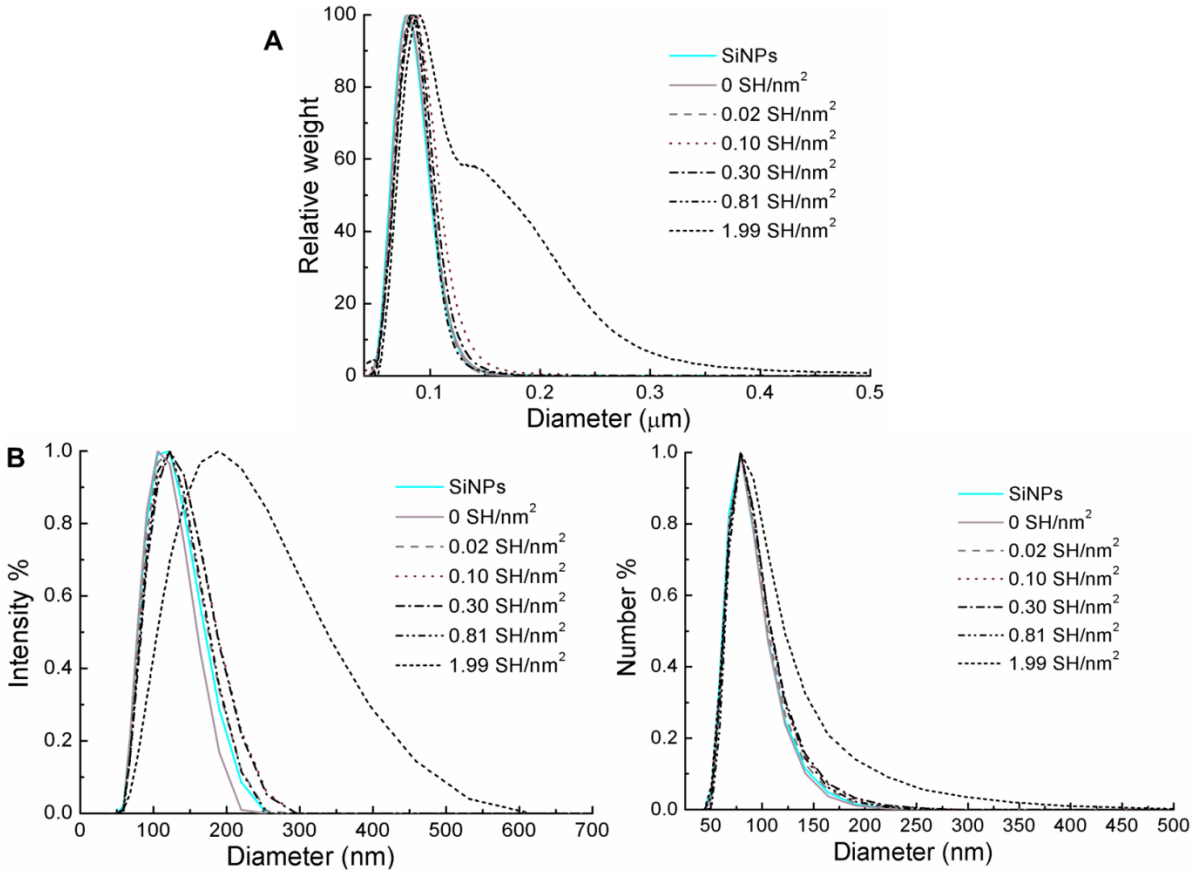

Figure S2: The apparent size of the thiolated SiNPs as determined using (A) DCS and (B) DLS.

S3: Size measurement of aminated SiNPs using (A) DCS and (B) DLS.

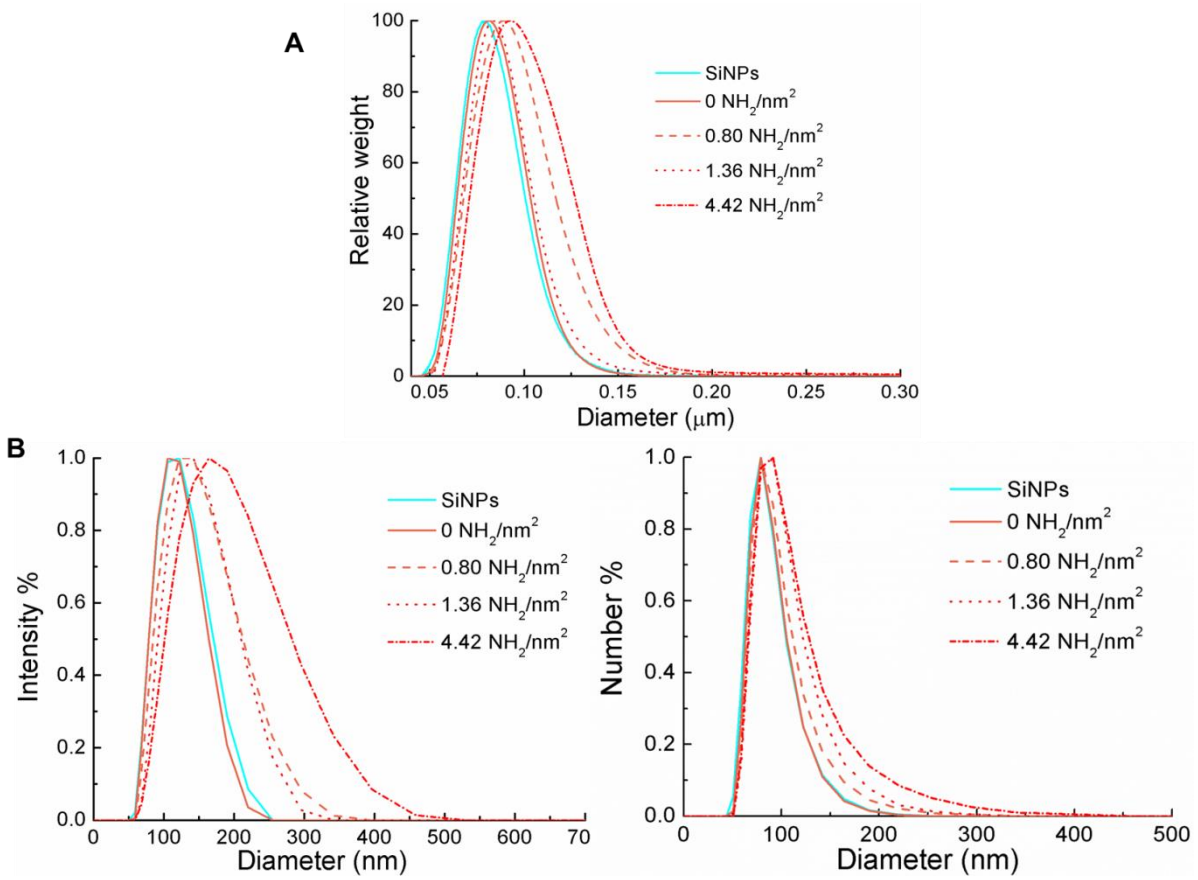

Figure S3: The apparent size of the aminated SiNPs as determined using (A) DCS and (B) DLS.

S4: Contrast between 0.8 nm and 1.4 nm AuNCs in TEM.

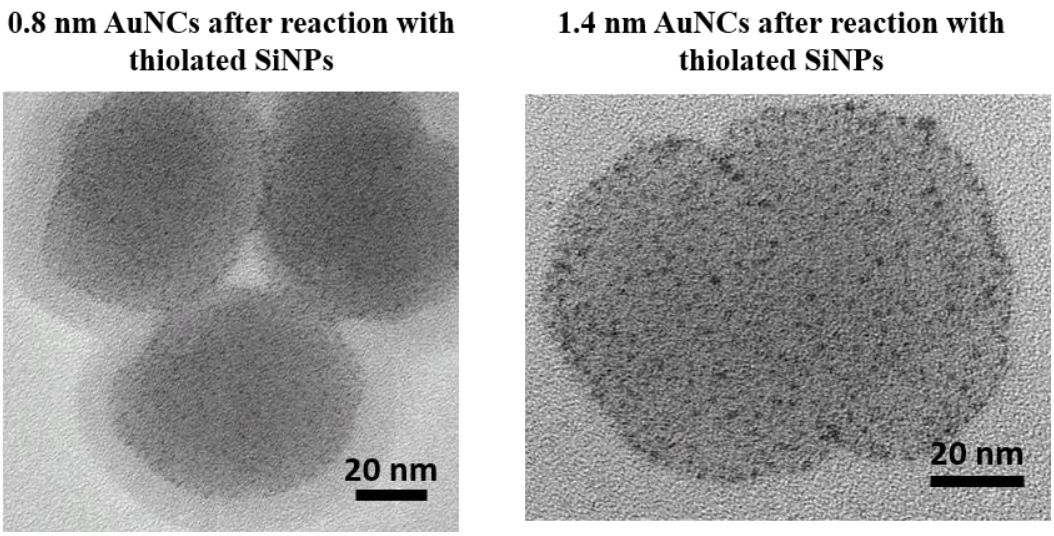

Figure S4: TEM image representing the contrast of 0.8 nm and 1.4 nm AuNCs on thiolated SiNPs and it can be observed that the 1.4 nm AuNCs are easier to be distinguished compared to 0.8 nm AuNCs and were thus selected for further experiments.

S5: Gel electrophoresis to investigate the monodispersity of AuNCs.

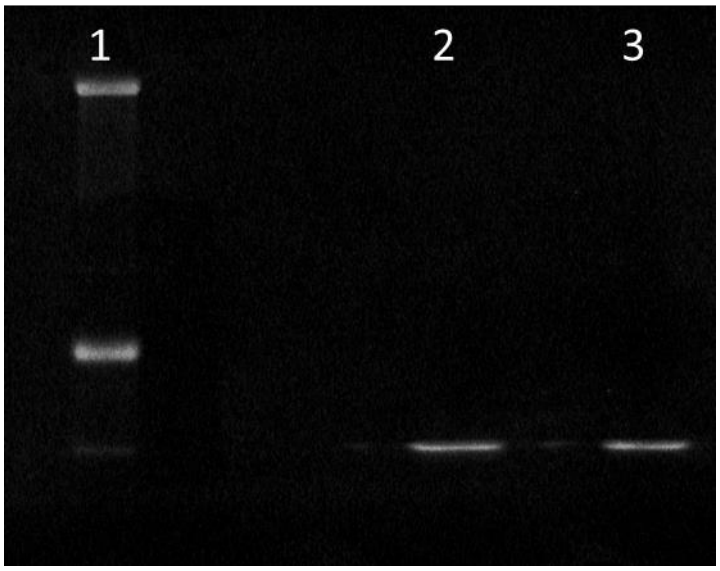

Figure S5: Gel electrophoresis of AuNCs to determine particle size distributions, where lane 1 is a protein ladder to act as a guide and reference. The lanes 2 and 3 are AuNCs done in two replicates, where a single band can be observed which confirms the high monodispersity of the AuNCs sample. DCS of the sample was also performed of AuNCs, where larger agglomerates were not observed (data not shown).

S6: Comparison of ratio of larger AuNCs with smaller AuNCs.

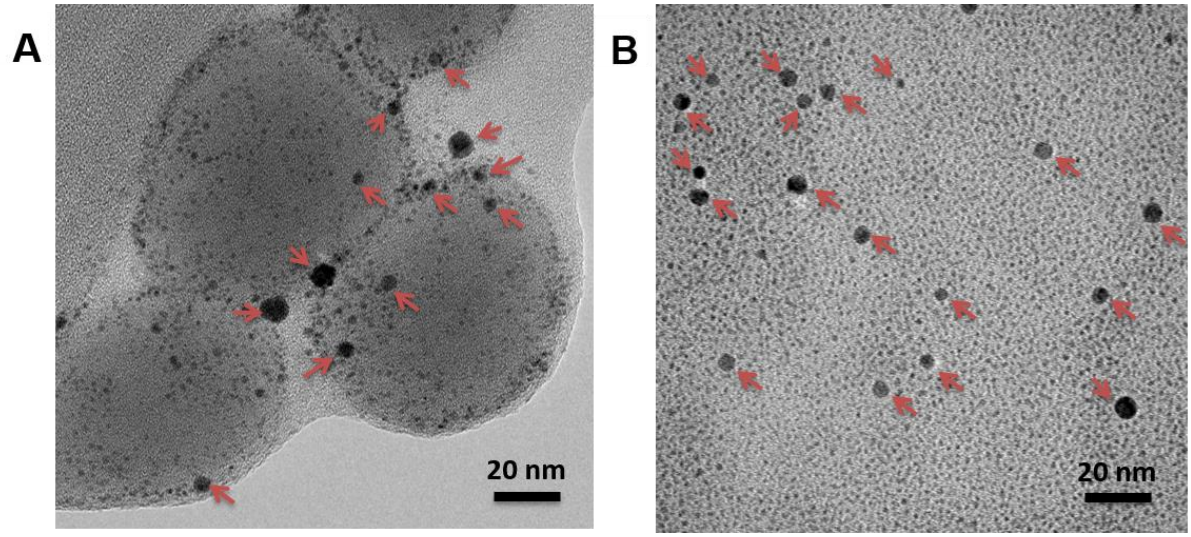

Figure S6: TEM image to show the presence of larger AuNPs in the sample of the AuNCs (approximately 1 for every 1000 small AuNCs) with an average diameter of 5.9 ± 2.1 nm represented by red arrows on the TEM images, which can be observed on the SiNPs with the majority of smaller AuNCs (1.4 nm). (A) On AuNC-mapped SiNPs and (B) without SiNPs (on a formvar/carbon copper TEM grid). Due to the low amount of larger AuNPs compared to the smaller AuNCs, the larger particles are suggest not to influence the mapping procedure significantly. If necessary, they might be removed in an additional size selection step.

S7: TEM image of contrast of AuNCs on SiNPs.

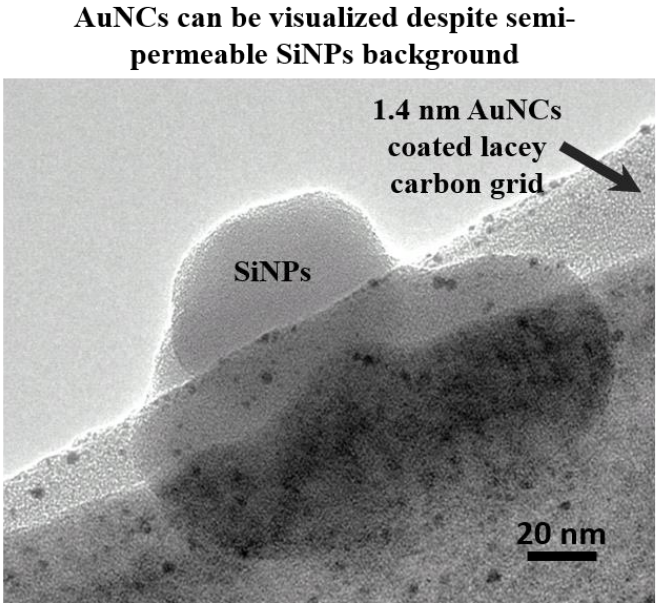

Figure S7: TEM image representing the contrast of AuNCs on SiNPs. To examine the contrast of AuNCs in TEM, a drop of AuNCs was casted onto a carbon grid and dried which was later top-layered with a drop of SiNPs. It is observed that AuNCs are clearly visible even with a layer of SiNPs on the AuNCs. This will facilitate us to examine AuNCs that are on the entire surface of the SiNPs.

S8: Reverse Ellman's assay to determine the number of maleimide groups on Mal – AuNCs.

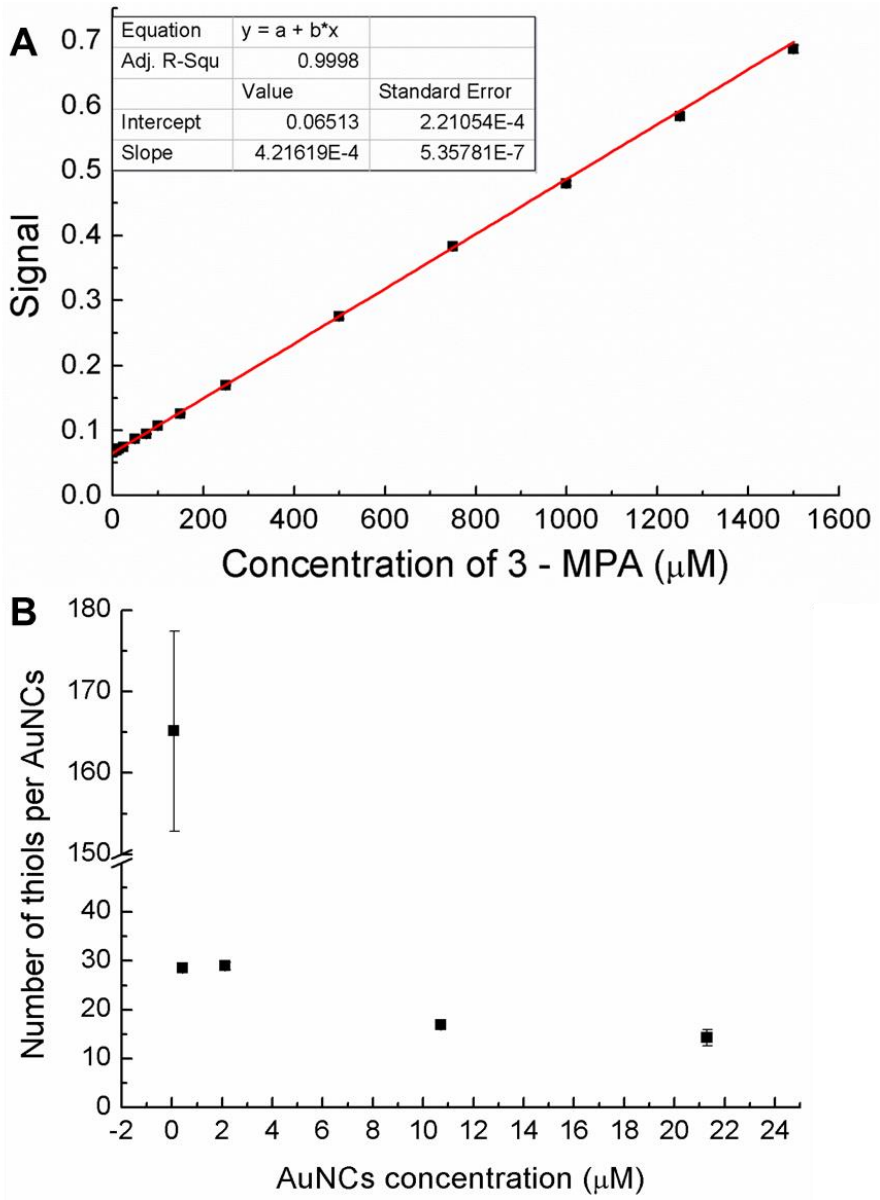

Figure S8: Reverse Ellman's assay was used to determine the number of maleimide groups on the AuNCs. (A) A calibration curve was done using 3 – mercaptopropionic acid (3-MPA), with an initial concentration of 1500 μM (Figure S8A). Using the calibration curve, the number of thiols consumed by maleimide on the AuNCs was calculated. For this purpose, 5 different dilutions of the Mal – AuNCs was reacted with a specific concentration of 3 – MPA and was back calculated to establish the number of maleimide present per AuNCs. (B) Varying concentrations of AuNCs were reacted with 3 – MPA and Ellman's assay was used to examine these samples. From Figure S8B, the

first and last dilutions were neglected due to the high error. The 3 dilutions illustrate that around 15 – 30 thiols react with one AuNCs. This can only be explained if there is more than one maleimide group present per AuNCs or the thiol of the 3 – MPA is reacting with the gold surface. The surface area of these 1.4 nm AuNCs can be calculated to be 6.16 nm^2 and it has been found that 4 – 6 thiols can bind per nm^2,[2] which corresponds to 25 – 37 thiols binding per AuNCs. But the thiols on the SiNPs are fixed and cannot access the AuNCs' surface as the thiols of the 3 – MPA, and hence will have a lower binding efficiency and significantly lower the probability for an interaction with the Au surface. On a highly thiol saturated SiNPs' surface, an AuNCs with an area of 1.54 nm^2, can occupy up to 8 – 10 silane groups. Thus from this measurement we can conclude that an AuNCs has the capacity to bind about 15 – 30 thiols **and we expect that on the surface of a particle, a maximum of ~5 – 7 thiols are occupied by one AuNCs depending on the density of thiols on the surface of the SiNPs. Nevertheless, such a replacement reaction is unlikely as the AuNC surface is covered by maleimide which would (if they not react first with the thiol) be stripped/replaced first and we suggest that the process does not influence thiol-specific AuNC-mapping.**

S9: TEM image of AuNCs labelled thiolated SiNPs.

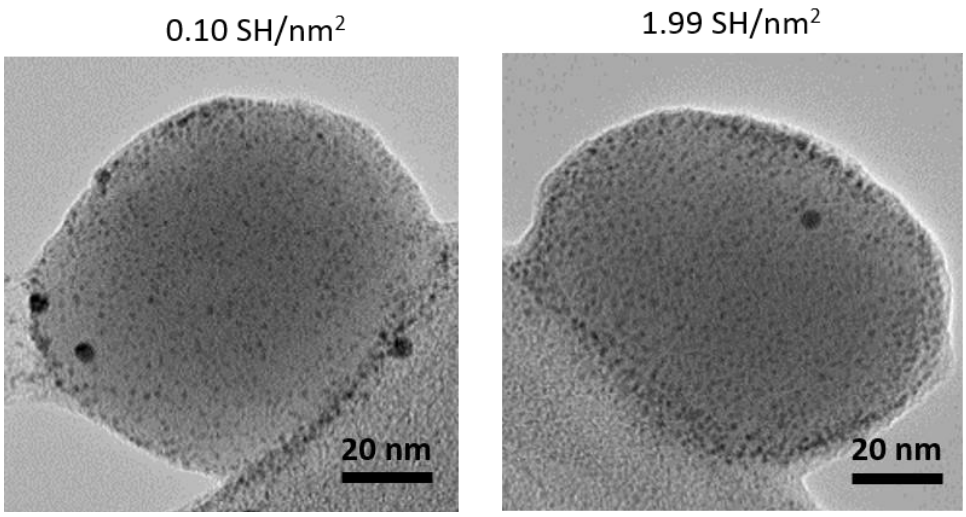

Figure S9: TEM image of Mal – AuNCs labelled thiolated SiNPs for 2 further thiol concentrations.

S10: Distance measurements of mapped samples between the functional groups for (A) thiolated and (B) aminated SiNPs.

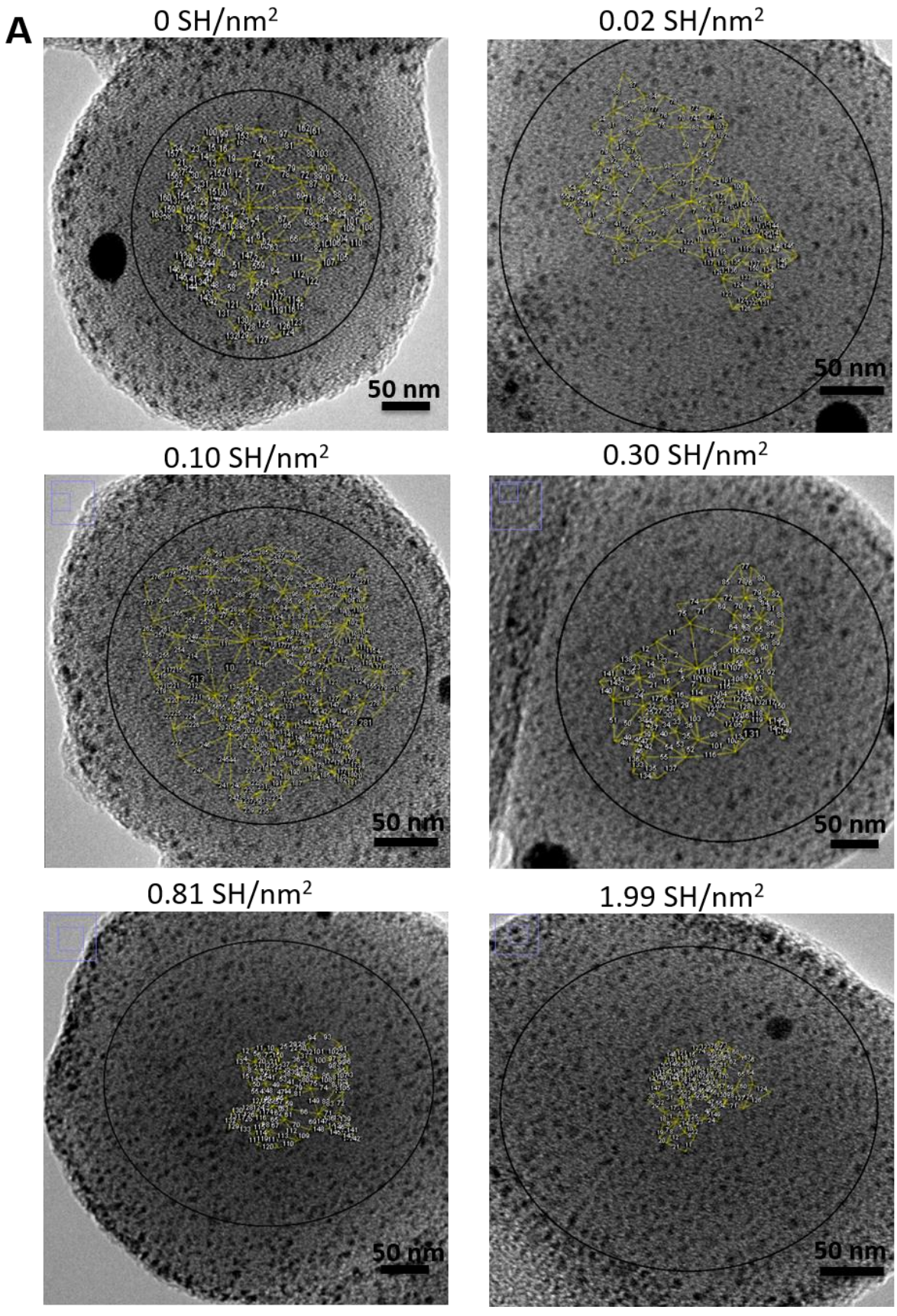
A
0 SH/nm2
0.02 SH/nm2
0.10 SH/nm2
0.30 SH/nm2
0.81 SH/nm2
1.99 SH/nm2
50 nm

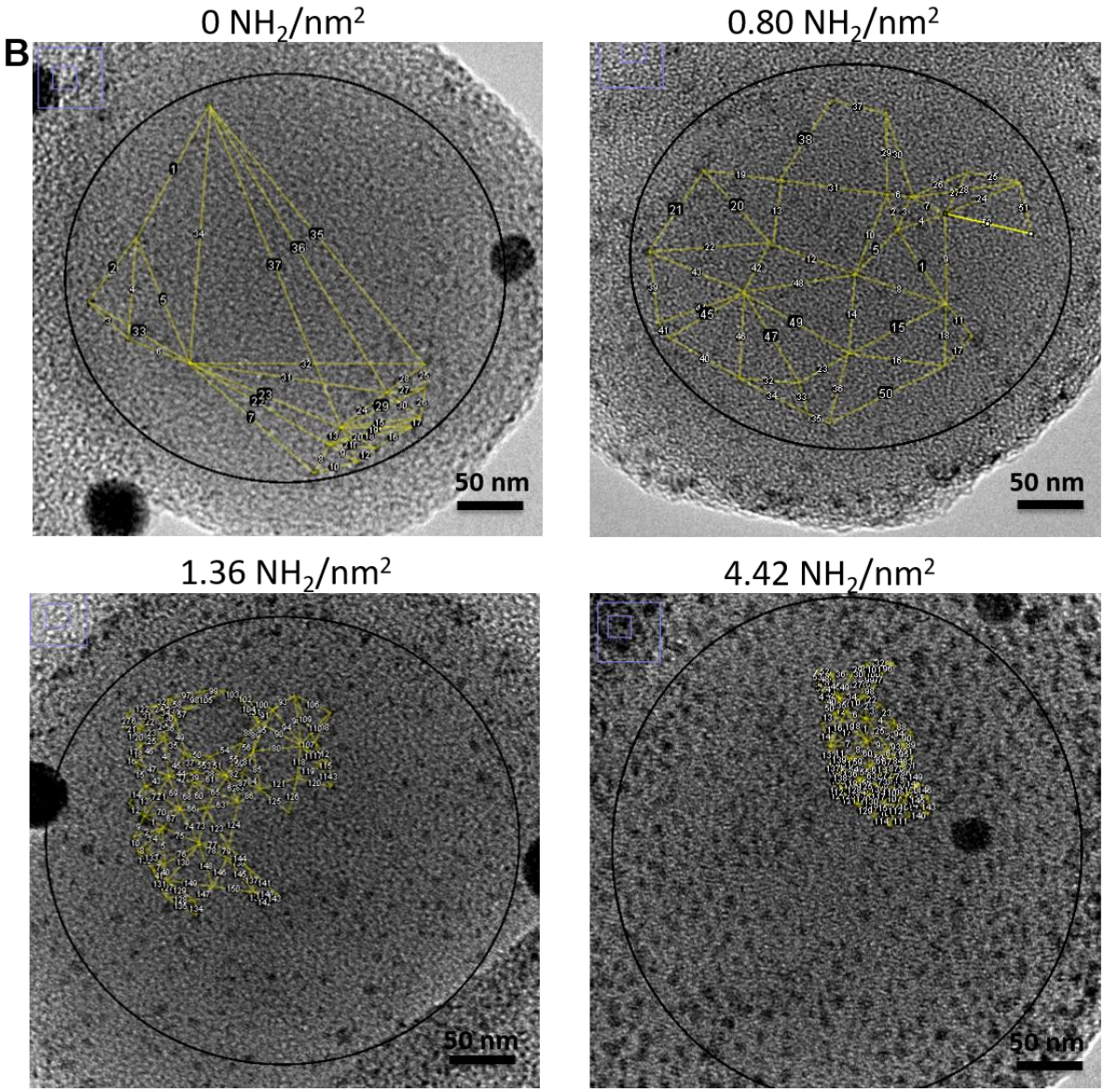

Figure S10: TEM microscopy mapped images of varying concentrations of thiolated and aminated SiNPs. A circular region with a diameter of 60 – 70 nm was selected such that the periphery of the SiNPs was avoided. The distance measurement was performed using Image J software (Version 1.47v) where for each images a minimum of 100 distance measurements were done and was done in triplicates. The yellow lines on each images represents the distance between each AuNCs. (A) Distance measurement for thiolated SiNPs which were mapped using Mal – AuNCs and (B) aminated SiNPs mapped with NHS – AuNCs, for varying surface density of functional groups.

S11: Reaction scheme of sintering steps with corresponding TEM images

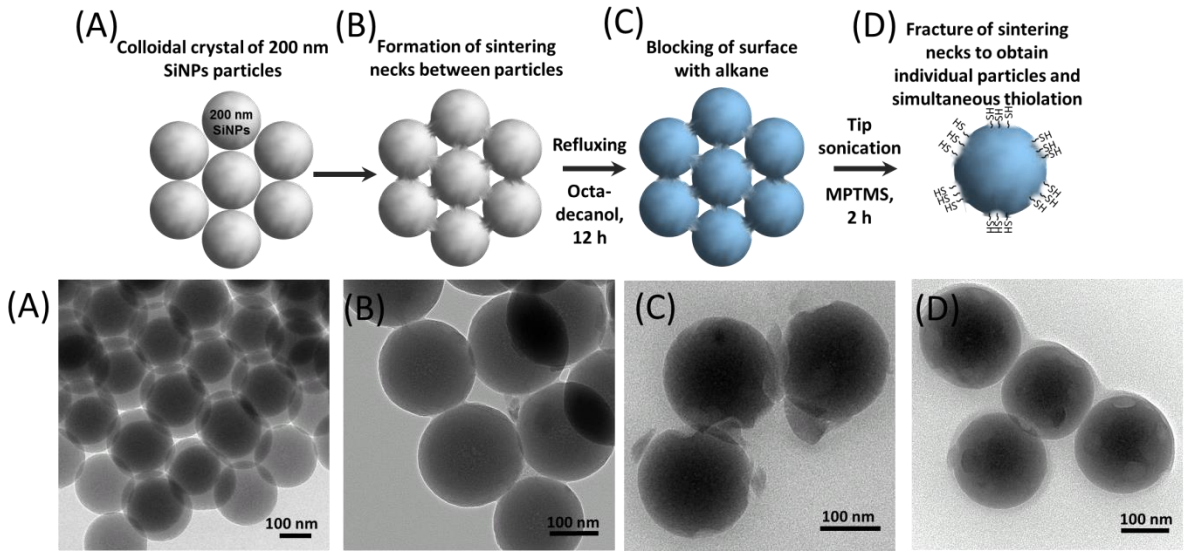

Figure S11: Illustrations and TEM images corresponding to the synthesis steps of SiNPCC by sintering 200 nm SiNPs, followed by thiolation to obtain patches of thiol groups on the surface. The thiolation was confirmed by mapping with Mal – AuNCs as explained in the main manuscript.

S12: Ellman's assay: Blocking of SiNPs with ZnO and IO NPs.

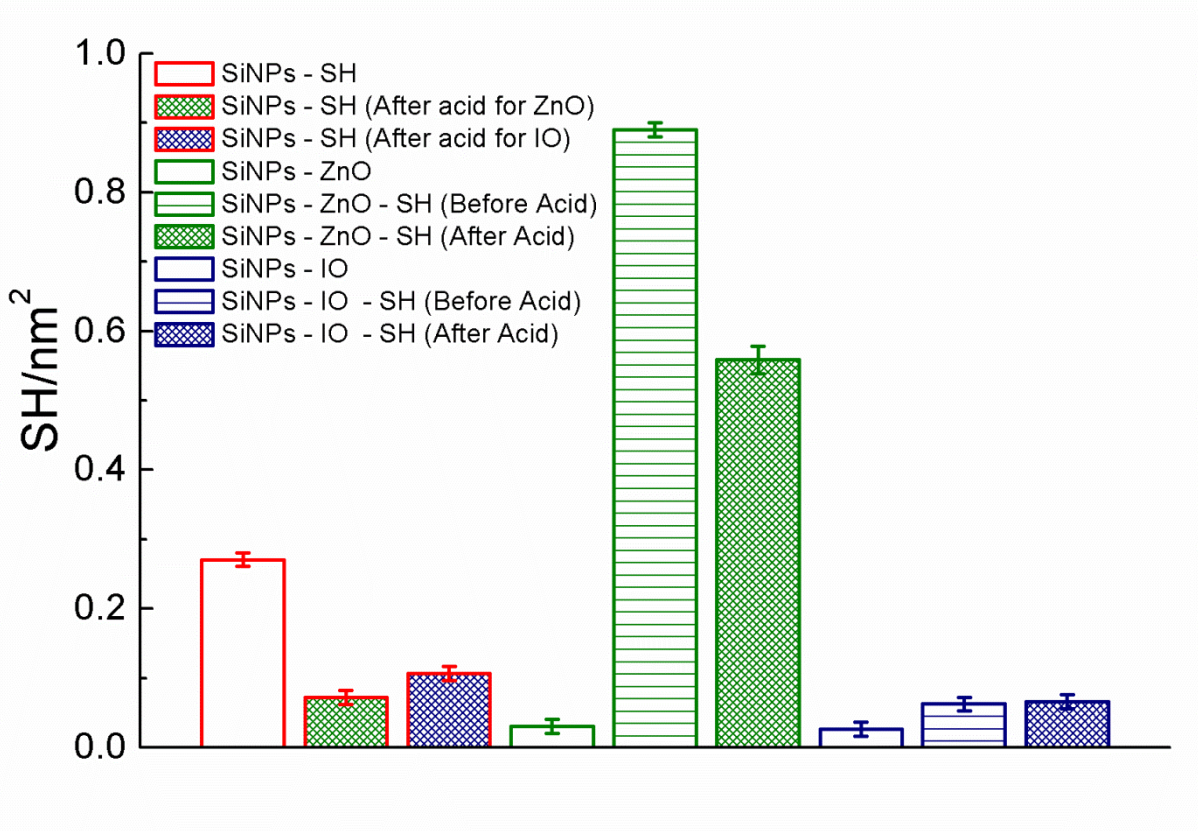

Figure S12: Ellman's assay to determine the effect of acid treatment on thiol functional groups during surface blockage using ZnO and IO NPs. From the graph, the first three data points (red outline) illustrate number of SH/nm^2 for the thiolated SiNPs without any surface blockage. The first data bar illustrates thiolated SiNPs without any acid treatment and the subsequent two data points indicates the thiolated SiNPs after acid treatment respectively for ZnO (0.06 M HCl) and IO NPs (3 M HCl), from which it can be observed that there is a decrease in the amount of thiol groups per nm^2. This illustrates that there can be a slight effect of acid on the thiol groups and which can also be due to detachment of loosely bound thiol groups from the surface during the washing step to remove the acid before the photometric assay.

For the next three data points (green coloured), the first data point illustrates bare SiNPs that have been adsorbed with ZnO NPs but not thiolated (to act as a reference), subsequently utilized for the Ellman's assay and the signal from the photometric assay is very low since the surface does not have any thiol groups. For the next two data points, the initial data corresponds to SiNPs coated with ZnO, followed by thiolation before acid treatment and

second corresponding to after acid treatment with 0.06 M HCl to remove the ZnO NPs. Thus on comparing that we can observe that the before acid treatment comprises more thiol groups, since the thiol groups can also bind on to the ZnO NPs and hence giving a higher signal in the assay. After the acid treatment, as the ZnO are removed resulting in decreased number of SH/nm^2.

The last three data points (blue coloured) on the figure represents the IO NPs blocked SiNPs' surface, the initial data point presents SiNPs with IO NPs without any thiols on the surface (reference particles), hence the low photometric signal. The last two points signifies the effect of acid treatment on the IO blocked SiNPs before and after acid treatment respectively, where both data points have a low signal which can be due to low concentration of thiol on the surface and below the detection limit of the assay (detection limit of Ellman's assay is 50 μM).

3 References

1. Adamczyk, Z., *Particles at Interfaces: Interactions, Deposition, Structure*. 2006.
2. Hinterwirth, H.; Kappel, S.; Waitz, T.; Prohaska, T.; Lindner, W.; Lämmerhofer, M., Quantifying Thiol Ligand Density of Self-Assembled Monolayers on Gold Nanoparticles by Inductively Coupled Plasma–Mass Spectrometry. *ACS Nano* **2013,** *7*, 1129-1136.